PROCESSING AND CHARACTERIZATION

OF UNIDIRECTIONAL THERMOPLASTIC NANOCOMPOSITES

by

KAMESHWARAN NARASIMHAN

A DISSERTATION

Submitted in partial fulfillment of the requirements
for the degree of Doctor of Philosophy
in the Department of Aerospace Engineering and Mechanics
in the Graduate School of
The University of Alabama

TUSCALOOSA, ALABAMA

2009

Copyright Kameshwaran Narasimhan 2009
ALL RIGHTS RESERVED

ABSTRACT

The manufacture of continuous fibre-reinforced thermoplastic nanocomposites is discussed for the case of E-Glass reinforced polypropylene (PP) matrix and for E-Glass reinforced Polyamide -6 (Nylon-6), with and without dispersed nanoclay (montmorillonite) platelets. The E-Glass/PP nanocomposite was manufactured using pultrusion, whereas the E-Glass/Nylon-6 nanocomposite was manufactured using compression molding. Mechanical characterization of nanocomposites were performed and compared with traditional microcomposites. Compressive as well as shear strength of nanocomposites was improved by improving the yield strength of the surrounding matrix through the dispersion of nanoclay. Significant improvements were achieved in compressive strength and shear strength with relatively low nanoclay loadings. Initially, polypropylene with and without nanoclay were melt intercalated using a single-screw extruder and the pultruded nanocomposite was fabricated using extruded pre-impregnated (pre-preg) tapes. Compression tests were performed as mandated by ASTM guidelines. SEM and TEM characterization revealed presence of nanoclay in an intercalated and partially exfoliated morphology. Mechanical tests confirmed significant improvements in compressive strength (~122% at 10% nanoclay loading) and shear strength (~60% at 3% nanoclay loading) in modified pultruded E-Glass/PP nanocomposites in comparison with baseline properties. Uniaxial tensile tests

showed a small increase in tensile strength (~3.4%) with 3% nanoclay loading. Subsequently, E-Glass/Nylon-6 nanocomposite panels were manufactured by compression molding. Compression tests were performed according to IITRI guidelines, whereas short beam shear and uni-axial tensile tests were performed according to ASTM standards. Mechanical tests confirmed strength enhancement with nanoclay addition, with a significant improvement in compressive strength (50% at 4% nanoclay loading) and shear strength (~36% at 4% nanoclay loading) when compared with the baseline E-Glass/Nylon-6. Uni-axial tensile tests resulted in a small increase in tensile strength (~3.2%) with 4% nanoclay loading. Also, hygrothermal ageing (50 °C and 100% RH) of baseline and nanoclay modified (4%) E-Glass/Nylon-6 was studied. It was observed that the moisture diffusion process followed Fickian diffusion. E-Glass/Nylon-6 modified with 4% nanoclay loading showed improved barrier performance with a significant reduction (~30%) in moisture uptake compared to baseline E-Glass/Nylon-6 composites. Significant improvement in mechanical properties was also observed in hygrothermally aged nanocomposite specimens when compared with the aged baseline composite.

DEDICATION

This dissertation is dedicated to my beautiful wife, Vinitha. Your love, support and patience encouraged me to complete this dissertation. You are my number one.

ACKNOWLEDGMENTS

I would like to sincerely thank Dr. Samit Roy for his guidance and patience during my doctoral program. I am grateful to him for offering me to continue with my research and move with him to the University of Alabama, Tuscaloosa. It has been a great learning experience working with him. He has constantly encouraged me giving me the drive to attain set goals, the independence to work and develop individuality. His mentorship was paramount in providing a well rounded experience.

I express my sincere thanks to my committee members Dr. Mark E. Barkey, Dr. Anwarul Haque, Dr. Mark L. Weaver and Dr. Jialai Wang for their invaluable insights and guidance. They have always been supportive and encouraging with the counseling of the dissertation.

I would like to acknowledge Dr. Chris Brazel and his research group for their time and support with various thermal characterizations. Also, I would like to thank Farzana Hussain, for her work and contribution to my dissertation. I appreciate the cordial help and support of all staff members of AEM and machine shop. I would like to extend my thanks to my research group for their wonderful conversations, support and understanding.

Most importantly, I would like to thank my wife, Vinitha. Her patience, support, encouragement, and unwavering love are undeniable in the past three and

a half years of my life. She has always challenged me intellectually and eager to help me with my research. She has been my enduring source of joy and strength. She has been wonderfully understanding throughout the dissertation process and to her I dedicate this dissertation.

I would also like to thank my parents, Narasimhan and Gayatri, my in-laws Krishnamurthy and Lakshmi, my brother Viswesh, my sister in-law Krithika and my *patti*, Janakavalli. They have unconditionally supported and encouraged me with their best wishes.

CONTENTS

LIST OF TABLES

LIST OF FIGURES

CHAPTER 1

INTRODUCTION

Polymer Matrix Composites (PMCs) have evolved and gained prominence over metals due to their specific strength, specific stiffness, corrosion resistance, acoustical dampening and tailorability. The versatility of the material is also enhanced with the wide range of choice available for the types of reinforcement and matrices to meet the demands in engineering, biomedical and other applications.

A composite structure is a combination of two or more different constituents, which can be physically distinguished, resulting in a final product having better performance than each individual constituent. Fiber reinforced polymer composites exhibit high specific strength, specific stiffness and corrosion resistance compared to conventional metallic components. They have gained prominence over traditional materials with their versatility and superior performance, thus widely being preferred in aerospace, automotive, marine and sporting applications. There has been a steady growth in aerospace applications to which PMCs are well suited. The Boeing 787 Dreamliner takes advantage of advanced composite materials by using 50% of polymer composites by weight in its design. Carbon Fiber-Reinforced Polymer (CFRP) is predominately used in advanced aerospace applications.

In a CFRP the fibers serve as a load-carrying member. The matrix protects the fibers from the environment and also acts as a load transfer medium between fibers. In less ideal cases where

the loads are complex, matrix may even have to bear loads transverse to the fiber axis. Polymer matrices are classified in two categories: thermosetting and thermoplastic. The polymer molecules in thermoset polymers are crosslinked due to the chemical reaction during the curing process. Once crosslinked, thermoset resins are permanently set and tend to chemically decompose at elevated temperatures. Thermoset polymers possess better dimensional stability and abrasive resistance than thermoplastic polymers. Thermoplastic polymers, on the other hand, have better post-process formability, enabling it to be reformed with the application of heat and improved repairability. Also, thermoplastics exhibit superior chemical resistance, fracture toughness and impact resistance than thermoset polymers. Often, however, the inherent properties of the polymer alone are insufficient to meet the structural demands of an application. As a result, blending with a stronger or stiffer material is necessary to improve upon the mechanical performance of the pristine polymer.

The fiber-matrix interfacial adhesion plays an important role in determining the mechanical properties of a PMC, Chen and Curliss (2001). In general, a better interfacial bond will impart better properties to a fiber reinforced composite, Jang (1994). While the in-plane, fiber-dominated properties (for example tensile strength) make these composites highly desirable as compared with metals, their thickness direction (or Z-axis) properties are limited by the performance of matrix resin. However, their compressive strength is generally much lower due to the fact that under compression, the fibers tend to fail through buckling well before compressive fracture occurs. In addition, fiber misalignment and presence of voids during manufacturing processes contributes to a further reduction in compressive strength. In fact, the overall compressive strength of a polymer matrix composite is only about 50% of its tensile

strength. The strength of the surrounding polymer matrix plays a key role in characterizing the critical buckling load of the fibers by constraining the fibers from buckling.

1.1 Thermoplastic and Thermoset Composites

Fiber-reinforced composites with thermosetting or thermoplastic matrices have been successfully used as engineering materials. This is primarily due to the improved mechanical properties of the composites compared to the monolithic matrix material. The better mechanical properties of the fiber-reinforced composites are a direct consequence of the properties of reinforcements such as glass, aramid or carbon fibers. Fiber-reinforced composite materials show better mechanical properties than most metals and hence have replaced them in a wide range of applications. In addition to their improved mechanical properties, they offer attractive benefits like low weight and resistance to corrosion.

Fiber-reinforced thermoplastic composites use a thermoplastic polymer as a matrix. Thermoplastics polymers are long chain polymer varying from medium to high molecular weight polymer and either semi-crystalline or amorphous in structure. In thermoplastic composites, the thermoplastic polymers used can be classified into two groups, namely engineering thermoplastics and high temperature thermoplastics. The classification is based on the maximum service temperature of the polymer composites. This temperature is dictated by the Glass Transition (T_g) temperature. This is the temperature at which the amorphous portion of the thermoplastic polymer changes from a glassy to a rubbery phase on heating. Typically, semi-crystalline thermoplastic polymers have the ability to carry load above T_g, because only the amorphous phase of the polymer has become rubbery. The crystalline portion of the polymer

remains solid until the melt temperature, T_m unlike thermoset composites, because thermoset polymers may not carry mechanical loads above T_g.

Thermoset polymers are widely used as structural composites. One of the biggest advantage of thermoset polymers from a processing stand point is that they have a very low viscosity and hence can be infused into fibres at low pressures. The fiber impregnation is followed by chemical curing to give a solid structure, which can usually be carried out isothermally as in Resin Transfer Molding (RTM). Thermoplastics on the other hand can be molded non-isothermally to achieve faster cycle times, i.e. a hot melt injected into a cold mold. However, polymerized thermoplastics tend to have melt viscosities between 500 to 1000 times that of thermosets, which necessitates higher pressures resulting in processing difficulties and increased expenditure in terms of tooling and energy input in heating and cooling the tooling. These disadvantages have in many cases outweighed the advantages of thermoplastic materials such as ease of recycling and high impact toughness, and limited their applications. Even though thermoset composites are easier to process, requiring less energy and pressure; they are inherently brittle and cannot be efficiently recycled. Also, there are significant environmental issues associated with thermoset processing, because a chemical reaction is necessary to form the solid structure of the polymer. Approximately 65% of thermoset matrices used in structural composites are unsaturated polyesters. Environmental regulations regarding the styrene emissions of unsaturated polyester are affecting the total cost associated with using them. Consequently many manufacturers are willing to consider a surrogate for unsaturated polyester even at a higher cost penalty.

Recyclability is becoming increasingly important in many sectors, especially in the automotive market. As mentioned earlier, thermoplastic composite polymers can be readily recycled; an

advanced thermoplastic composite can be chopped into pellets and injection molded to yield long-fiber reinforced moldings, which can in turn be recycled at the end of their life. However, thermoset composite materials can only be ground and used as filler material thus decreasing the value of the composite. Thermoplastic composites have a niche market, primarily due to the difficulties in processing. Currently more than 90% of polymers used in composites are thermosets.

Lately, a new composites processing technology, known as liquid monomer processing, has been developed. This processing technique combines the advantages of thermoset processing to yield a polymer material with durability and environmental advantages of a thermoplastic polymer. In particular, one of the liquid monomer materials (Cyclics PBT) can be processed isothermally: i.e. the monomer is injected, polymerized, crystallized and de-molded at the same temperature. Thus the cycle time is limited by the injection, polymerization and crystallization time of the material.

1.2 Polymer Nanocomposites

Polymer nanocomposites are multi-component system, where the primary component is a polymer and the filler material has at least one dimension less than 100nm. Polymer nanocomposites require significantly lower filler loading to provide similar/or in certain cases higher property enhancements than realized with conventional fillers in traditional composites. This is primarily because of the increased surface area to volume ratio available at the nanoscale. There have been significant advancements in nanocomposite technologies as new classes of nanoscale fillers continue to emerge. Nanoparticles commonly dispersed in polymer matrices include: layered silicate clays, carbon nanotubes, Polyoctahedral silsesquioxane (POSS), carbon

nanofibers, and graphite nanoflakes. The morphology, aggregate size, chemistry and aspect ratio of the nano-fillers listed differ significantly.

The choice of nanofillers depends on the objective of the application. However, irrespective of the preference of nanofiller it is imperative that the nanofillers are compatible with the host polymer and well dispersed in the matrix to realize potential property improvements. In this research we examine the effect of addition of layered silicate clays on thermoplastic matrices. Layered silicate clays are composed of stacked nanosized platelets, which need to be delaminated into individual platelets in order to realize the nano effect. Working with these materials for high performance applications introduces issues that have not received significant attention in the literature, such as its effect on matrix yield strain in shear and in turn the compressive strength of the polymer nanocomposite, and moisture barrier effect due to the addition of layered silicates in the polymer matrix.

1.3 Layered Silicate Clay Nanocomposites

The layered silicate clay work has been separated into two sections with include effect on mechanical properties, such as the compressive strength and inter-laminar shear strength and the moisture barrier properties in polymer composites.

1.3.1 Mechanical Properties of Thermoplastic layered silicate clays

According to Argon (1972) and later Budiansky (1983), the critical buckling stress in the fiber is directly related to the stiffness and yield strain of the surrounding matrix material in shear, therefore any increase in these matrix properties would directly result in an improvement in the compressive strength of the composite. The yielding of the matrix would result in loss of matrix

stiffness in shear and eventually lead to local micro buckling and kink band formation, Budiansky and Fleck (1993), eventually leading to failure. Moreover, increase in composite longitudinal shear stiffness (G_{12c}) with nanoclay reinforcement can improve the compressive strength of the composite. Therefore it can be said that improving the yield strength and stiffness of the surrounding matrix in shear can improve the compressive strength. Also fiber alignment with process optimization, process control, and improved dispersion of nanoclay can play an important role in improving the compressive strength. There exist very little published data on the compressive strength of thermoplastic nanocomposites. Fibers in pultruded material are in general well aligned. However, the composite compressive strength is very sensitive to even slight misalignment in fiber orientation.

This work focuses on the improvement of compressive and inter-laminar shear properties of fiber-reinforced thermoplastic composites. This is accomplished by:

(1) Optimum dispersion of layered silicate clays in the host thermoplastic matrix with different weight addition

(2) Fabrication of fiber-reinforced polymer composite using the dispersed layered silicate clays

(3) Understanding the effect of different weight addition of layered silicate clay on the fabrication of fiber-reinforced polymer composite.

(4) Evaluating the compressive strength and inter-laminar shear strength of the fabricated fiber-reinforced polymer nanocomposites.

1.3.2 Moisture Barrier in Thermoplastic layered silicate clays

Thermoplastics have been widely utilized as a matrix resin for silicate clay nanocomposites, which are affordable and commercially available. The thermoplastic nanocomposites are primarily used for structural applications for its superior mechanical properties, such as in automobile or for its improved gas barrier properties, such as in packaging film applications. Similar to gas barrier properties, the moisture barrier properties with addition of silicate clay nanocomposites is significant due to the tortuous path created by the presence of dispersed layered silicates in the host polymer matrix. In this study, we attempt to answer the following questions with regard to moisture barrier effect with addition of layered silicate particles in a thermoplastic matrix;

(1) What is the effect on moisture diffusion with addition of layered silicate clays in different weight addition?

(2) What is the effect on total moisture uptake with addition of layered silicate clays in different weight addition?

(3) What is the underlying nanoscale mechanism of moisture barrier effect?

CHAPTER 2

OBJECTIVES

The overall compressive strength of a polymer matrix composite is only about 50% of its tensile strength. The strength of the surrounding polymer matrix plays a key role in characterizing the critical buckling load of the fibers by constraining the fibers from buckling. As mentioned earlier, the critical buckling stress in the fiber is directly related to the stiffness and yield strength of the surrounding matrix material in shear, therefore any increase in these matrix properties would directly result in an improvement in the compressive strength of the composite. Moreover, increase in composite longitudinal shear stiffness (G_{12c}) with nanoclay reinforcement can improve the compressive strength of the composite, Creighton and Clyne (2000) and Creighton *et al* (2001). Therefore it can be said that improving the yield strength and stiffness of the surrounding matrix in shear can improve the compressive strength. Also fiber alignment with process optimization, process control, and improved dispersion of nanoclay can play an important role for improving the compressive strength. There exist very little published data on the compressive strength of thermoplastic silicate layered nanocomposites. Also, the moisture barrier effect with addition of silicate layered clay to thermoplastic matrix is studied and an analytical model for the nano-scale diffusion mechanism is presented.

2.1 Mechanical properties of thermoplastic layered silicate nanocomposites

The compressive failure of continuous fiber reinforced composites has received considerable attention in the recent years because it typically occurs at a stress level that is 40-50 % below the

tensile strength of the composite. Earlier work by Rosen (1964), which assumed extensional (transverse) and shear microbuckling of the fibers embedded in an elastic matrix, consistently over predicted the compression strength when compared with experimentally measured values. Argon was among the first to recognize that fiber reinforced composites made by normal manufacturing processes, including pultrusion, have regions of fiber misalignment. Argon, and later Budiansky, showed that fiber misalignments present in fiber reinforced composites could lead to yielding of the polymer matrix in shear. The yielding of the matrix would, in turn, result in loss of matrix stiffness that could eventually trigger fiber microbuckling with resulting kink band formation, as shown in Figure 1.1, which could lead to final failure.

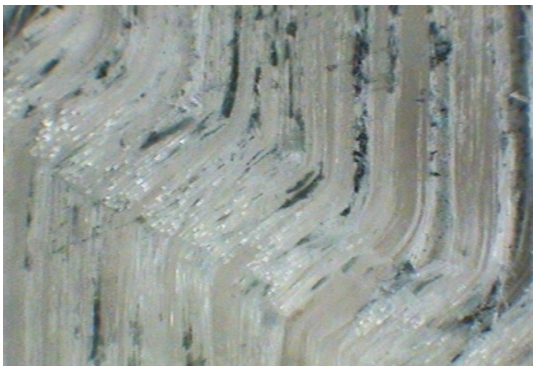

Figure 2.1 Compression failure of pultruded specimen showing kink band

Argon proposed a simple yet elegant formula for composite compression strength, σ_C , such that,

$$\sigma_C = \frac{\sigma_Y}{\phi_0} \qquad \text{-(1)}$$

where, σ_Y is the matrix yield strength in shear, and ϕ_0 is the initial fiber misalignment angle (in radians) with respect to load direction, sometimes referred to as fiber misorientation. Further, it is likely that any increase in composite shear stiffness (G_{12c}) due to the presence of nanoclay particles would result in an increase in the compressive strength of the composite, as indicated by

a modified form of the Argon formula that includes both elastic and plastic buckling behavior as limiting cases,

$$\sigma_C = \frac{1}{\left(\frac{1}{G_{12c}} + \frac{\phi_0}{\sigma_Y} \right)} \qquad \text{-(2)}$$

The failure mechanism described in Eqn. (2) is still a shear mode of fiber buckling, but unlike in Rosen's elastic analysis, it is the local nature of the imperfections, coupled with plastic yielding of the matrix in shear, that results in local buckling and kink formation visible in Figure 1. 1. From Eqn. (2), it quickly becomes apparent that improvements in the compression strength of the composite may be achieved by (a) improving the yield strength of the surrounding matrix in shear, and (b) reducing fiber misalignment in the composite through optimization of manufacturing process variables. The goal of this work is to improve the compressive strength and inter-laminar shear strength of unidirectional fiber-reinforced thermoplastic composites, by increasing matrix yield strength and decreasing fiber misalignment concurrently, thereby making use of synergies that may exist between these effects.

2.2 Moisture Barrier properties of thermoplastic silicate layered nanocomposites

The use of fiber-reinforced PMCs in advanced applications places numerous demands on the material. Even though, the primary function of the material is to provide structural strength, the mechanical properties are altered with exposure to environmental conditions, such as moisture. Prolong exposure to moisture will degrade material properties leading to failure of the structure. The addition of silicate layered clay to fiber reinforced PMCs can, in addition to enhanced mechanical properties, provide a superior product with a longer life and better moisture barrier

performance. A well dispersed silicate layered clay in a fiber reinforced PMC can result in a multifunctional material with excellent mechanical and barrier properties. Therefore, the moisture barrier effect with layered silicate clay nanocomposites and its underlying mechanism are investigated.

The addition of silicate layered clay nano-particles to polymer matrix has proven to be an effective mechanism to enhance the polymer matrix properties. Polymer silicate layered nanocomposites with a well dispersed morphology of nano-fillers can improve matrix strength, modulus, thermal stability, impact resistance, and barrier performance. Filler materials such as layered silicates, exfoliated graphite, POSS, silica, and carbon nanofibers and carbon nanotubes have been successfully dispersed in numerous polymer systems. The significant material property improvements with the addition of nano-fillers on various polymeric materials, such as thermosets, thermoplastics, rubbers, liquid crystalline polymers, copolymers, block copolymers, and polymer matrix composites have been reported. The nano-fillers can be made compatible with any polymer with appropriate functionalization of the nano-filler to fabricate and optimize polymer nanocomposites. The ability of silicate layered clays to impart significant improvement in mechanical and barrier properties depends on the compatibility of the nano-filler and the dispersion morphology. The purpose of this research is to demonstrate the improvement in compressive strength, inter-laminar shear strength, and the moisture barrier properties of thermoplastic silicate layered nanocomposites. We investigate the most commonly used layered silicate clay, montmorillonite (MMT) nanoclay. Two thermoplastic polymer matrices were chosen, polypropylene (PP) and polyamide 6 (PA6) or Nylon-6. In each case, the effect of addition of layered silicate clay are identified and optimized.

This dissertation is divided into two sections. Chapter 4 contains the results from studying the effect of layered silicate clay nanocomposites on the compressive strength and inter-laminar shear strength of the fiber-reinforced thermoplastic layered silicate nanocomposites. Chapter 5 contains the model description and results from studying the effect of layered silicate clay nanocomposites on the moisture barrier properties of the thermoplastic layered silicate nanocomposites and E-Glass fiber-reinforced thermoplastic layered silicate nanocomposites.

CHAPTER 3

REVIEW OF LITERATURE

In the early 1990s, Toyota researchers reported work on Nylon-6 nanoclay thermoplastic nanocomposites technology, Kojima *et al* (1993), Okada and Usuki (1995), and Usuki *et al* (1995). It has a broad-based proprietary patent technology that is licensed to companies in Japan and the USA, Christopher and Lerner (2001). The researchers observed a significant improvement in mechanical properties with clay loading of 4.2 wt% (weight%), with a 100% increase in modulus and more than 50% increase in strength properties. Further, an improvement in thermal properties was observed, with the increase of heat distortion temperature (HDT) by 80°C compared to the pristine polymer. In recent years, the use of organoclays as precursors for nanocomposite formation has been extended into various polymer systems. Polymer-matrix composites containing nanoclay (MMT) are an excellent example of where intrinsic nanoscale characteristics are the reason for superior properties. Addition of small amounts of nanoclay (~5%) significantly improves the stiffness, strength, gas barrier properties and fire-resistance properties of most thermoplastics, with only small effects on flexibility and optical clarity. Due to its low cost and availability, there is currently a great deal of focus on nanoclay fillers. These fillers are slightly more expensive than glass, yet generally much less expensive than carbon nanotubes.

Nanoclays are minerals with a high-aspect ratio and with at least one dimension of the particle-typically, the thickness in the nanometer range. Reinforcements in the nanometer size range

approach the size of the polymer molecule, enabling close interaction between the two materials. The proper chemical modification of nanofiller offers higher potential than unmodified nanofiller, to network with the polymer and creates constrained regions near the particle surface. This immobilizes a segment of the polymer chain, creating a reinforcement effect. Purity and cation-exchange capacity are two characteristics critical to the success of nanoclay as polymer-reinforcing agents. Purity is important in achieving maximum improvement in mechanical properties; impurities act as stress concentrators, resulting in poor impact and tensile properties. Cation-exchange capacity provides the surface activity necessary for acceptance of surface treatments to the nanoclay. Such treatments are essential to allow the nanoparticles to be compatible and be effectively dispersed in the polymer matrix.

The most important factor in the success of polymer reinforcement is the aspect ratio of the nanoclay platelet. Nanoclay platelets with a plate-like structure and a thickness of <1 nm are optimal. The length and width of these platelets are in the micron range, with aspect ratios between 300:1 to 1500:1. Nowadays, the various nanoclay nanofillers of commercial interest includes hydrotalcite, montmorillonite (MMT), mica fluoride, and octasilicate. Hydrotalcite and octasilicate have limits of use both from a physical and a cost standpoint. Mica fluoride is synthetic clay, while MMT occurs naturally.

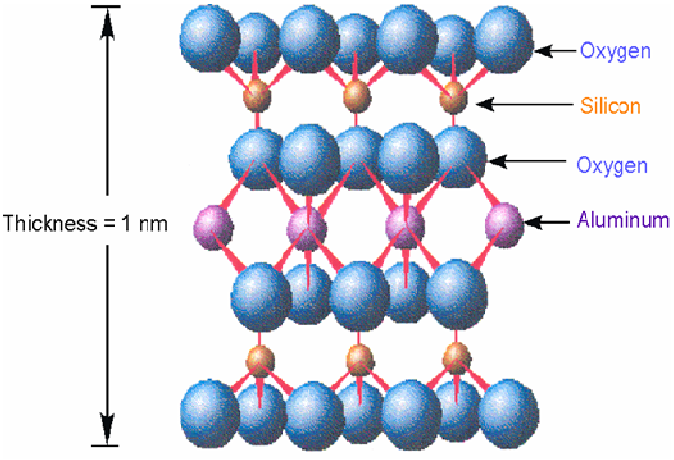

Figure 3.1 Structure of MMT nanoclay

MMT is most common and widely used nanoclay in polymers. MMT is

hydrophilic and belongs to the family of smectite clays with a unique feature of existing in agglomerates of nanoparticles platelets held together by attractive forces. MMT has a layered structure, with aluminum octahedron sandwiched between two layers of silicon tetrahedron, as shown in Figure 3.1. Each layered sheet is slightly less than 1 nm thin (10 Å), with surface dimensions extending to about 1 µm or 1000 nm. The aspect ratio is about 1000 to 1 and the surface area is in the range of 750 m^2/g. Because MMT nanoclay is hydrophilic, it is not inherently compatible with most polymers, especially thermoplastic polymers such as polypropylene (PP), Nylon6, etc. and must be chemically modified to make its surface more hydrophobic. The most widely used surface treatments (surfactants) are alkyl-ammonium cations, which can be exchanged for existing cations already on the surface of the clay. The role of the surfactant is to minimize the attractive forces between the agglomerated platelets, thereby enabling the polymer molecules to penetrate into the tactoid. Depending on the degree of polymer penetration into the silicate tactoid, two idealized nanocomposite structures are feasible: *intercalated and exfoliated*, shown in Figure 3.2.

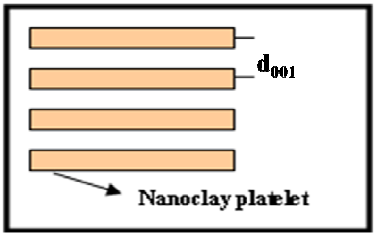

(a) Nanoclay platelets as agglomerates

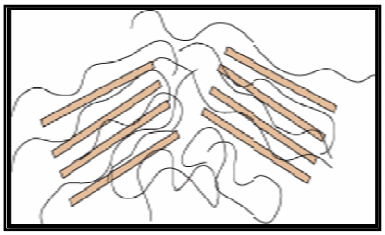

(b) Intercalated morphology

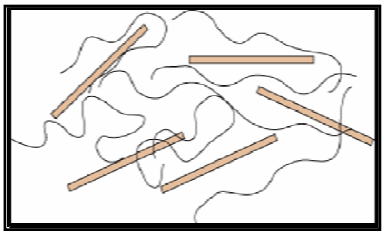

(c) Exfoliated morphology

Figure 3.2 Nanoclay morphology

The process of opening up the spaces between the clay platelets, thereby increasing the interlayer spacing or the gallery spacing (d_{001}) is called *intercalation*. The polymer molecules will not able

to penetrate into the galleries between the platelet layers without the process of intercalation. In the intercalated systems, the multi-layer structure of the silicates is retained, with alternating polymer/silicate layers and a repeat spacing larger than that of the original clay.

In *exfoliated* nanocomposites, the primary particles of the organically modified clay are delaminated into individual nanometer thick silicate platelets, which are subsequently dispersed uniformly in the polymer matrix due to extensive polymer penetration and intercalation. It is imperative that the nanoclays are intercalated in order to achieve exfoliation. As mentioned earlier, the thickness of the platelet is in the nanometer range, while the length and width are between 0.1 and 2 μm. Because of this, a single gram of exfoliated nanoclay will contain over a million individual particles with high total surface area.

Because nanofiller contains so many individual particles in such a small amount of material, it requires very low "loading" to obtain a high concentration of constrained areas within the polymer. Approximately, a 5 % of loading by weight of nanoclay often leads to reinforcing effect equal to about 12 to 15% glass fiber. The nanofiller also create a tortuous path for the penetration of gaseous vapors and liquids into the polymer. In turn, this leads to better chemical and environmental resistance.

Previously, most nanoclay research involved the incorporation of nanoclay into a polymer during the polymerization process, the so called in-situ polymerization method. With this method, exfoliation or dispersion of the clay particles is more efficient. But the batch sizes required for polymerization—and therefore the cost—has resulted in challenging economics for many commercial applications. To date, only a few commercially available compounds have been made using this method.

An alternative approach involves melt compounding the nanoclay and polymer. This method offers significant promise, since the modification of plastic compounds is a custom business and well suited for manufacturing applications. In combination with the pretreatment of the clay itself, the compounding parameters and mixing-screw profile are important variables. Since the clay is an aggregate of thousands of individual platelets, it is critical that those platelets be exfoliated prior to compounding. If the platelets are not separated, it is unlikely that the shear forces generated during the compounding process will be sufficient to overcome the forces holding the aggregates together. Hence optimum exfoliation or dispersion cannot be attained. The right clay treatment is required to allow for intercalation and exfoliation; after that, it is necessary to make the intercalate compatible with the host polymer so some properties are enhanced without sacrificing others. This allows for improvement in the strength without embrittlement of the polymer resin. Secondly, melt compounding must occur such that the prepared clays get maximum dispersion without degrading the polymer. Today, several nanoclay compounds are commercially available and have been used successfully.

Ultrasound sonication is another method widely employed for dispersion of silicate layered clays in the host polymer matrix. Sonication imparts energy to the silicate platelets to break the restraint force from the stack of platelets. The energy, provided in the form of high frequency vibrations, not only helps the silicate platelets to break from the stack as individual platelets, but also aids in moving the platelets in the polymer/nanoclay mixture. It is critical to optimize the sonication energy and time because high energy can break the platelets thus reducing the aspect ratio and extended sonication times can result in re-agglomeration of platelets, which is undesirable to achieve improved properties.

The dispersion of silicate layered clays in thermoset resins are primarily performed using a high shear mixer. The surfactant modified silicate platelets is mixed in the resin (before adding the hardener) at very high shear rates (2000 - 4000 rpm) for extended period of time, typically for 1-2 hours. This would facilitate the dispersion of layered silicates in the resin prior to curing with hardener. Studies reveal that combined effect of high shear mixing followed by sonication can play an effective role in dispersion silicate layered clays in thermoset resin systems.

As mentioned previously, addition of small amounts of clay (~5 wt%) significantly improves the mechanical properties and barrier properties and fire-resistance properties of most thermoplastics, such as PP, Nylon-6 etc., with only small effects on flexibility and optical clarity. Vlasveld *et al* (2005) observed that PA6 nanocomposites absorb water at a slower rate than the unfilled PA6 specimens. The diffusion coefficients of the nanocomposites are reduced to approximately 1/3rd of the original value at the highest silicate loading. The conditioning temperature strongly influenced the time needed to reach saturation. The degree of exfoliation influenced the properties of PA6 nanocomposites. The authors noted that the modulus of the PA6 nanocomposites increased continuously with increasing silicate content; at around 10 wt % the moduli of the Cloisite and Nanomer nanocomposites were twice that of the unfilled PA6 resin. At higher silicate content the modulus increase levels off of the PA6 nanocomposite, while the Somasif MAE nanocomposites had a lower modulus at all concentrations due to reduced exfoliation. Further the authors found that the modulus of moisture-conditioned nanocomposites showed a reduction just like the unfilled polymer. At around 6% silicate the modulus of the moisture conditioned nanocomposite is equal to the modulus of the dry unfilled polymer (at

room temperature). Also, the fracture behavior of the nanocomposites is influenced by the type and concentration of the nanofiller, the moisture content and the aging time.

The addition of silicate layered nanoclay creates a tortuous path for any permeant into the polymer because the nano-filler is impenetrable. Nielsen (1967) proposed a simple two dimensional theory for polymer nanocomposites. The theory accommodates the tortuosity due to addition of layered silicates and the aspect ratio of silicate platelets. This model predicts the vapor permeability for low silicate nanoclay loading and deviates significantly at higher silicate nanoclay loadings for certain type of polymers. Sorrentino *et al* (2006) proposed a geometric model to predict the effective diffusivity in polymer nanocomposite thin films as a function of silicate clay platelet orientation, volume fraction, clay-polymer interaction and the aspect ratio of the platelets. The proposed model considered the tortuosity and the interface regions developed between the polymer and the silicate clay due to surface modifications of the nano-filler. Thus a geometric hindered factor and a vacancy factor were used in the proposed model to predict diffusivity of polymer nanocomposites. However, the idealized assumption that the silicate clay platelets were all oriented in the same direction cannot be extended to bulk polymer systems, albeit true in most polymer films. Liu et al (2007) had developed a three dimensional model for the water-uptake behavior in epoxy-clay nanocomposites. Diffusion models were developed to predict the diffusivity of polymer nanocomposites for an intercalated and an exfoliated nanocomposite system.

Adame and Beall (2009) theorized that the constrained polymer region extends 50 to 100 nm away from the surface of the clay and confirmed it by an analysis preformed through Atmoic

Force Microscopy (AFM). Further it is evident that the constrained region of semicrystalline polymers will not significantly affect permeability unless the overall crystallinity is decreased. The main effect of the constrained region is to lower free volume. That will not be significant in crystalline region which also explains the reason crystalline polymer nanocomposites fit the simple tortuous path predictions reasonably well. In contrast amorphous polymers should exhibit the largest effect of constrained polymer regions due to reduction in free volume. Most of the large deviations from the simple tortuous path model that have been reported in the literature involve amorphous polymers. The fundamental origin of the lowered diffusion rates in this constrained region could also be related to lowered solvent uptake due to the polymers being restricted in its ability to move. Restriction of polymer motion is a function of the interaction of the polymer with the surface of the nanoparticle. This proposed mechanism is supported by observations of solvent uptake by Burnside and Giannelis (2000), Liang and Yin (2003), Liang et *al* (2004), Singh and Mukherjee (2005), Promanik *et al* (2004) on a number of nanocomposites. In each of these cases the solvent uptake decreased with increasing nanoparticle loading and was substantially lower than the solvent uptake of the pure polymer. The large changes observed in solvent uptake in these nanocomposites provide strong indirect evidence of the constrained polymer region and its size. In the work on solvent uptake by ethylene–vinyl acetate nanocomposites, the solvent uptake effect levels off at around 5% by weight of clay nanoparticles. This indicates that nearly all the polymer in the composite is constrained at this nanoclay loading level. At 5% by weight assuming that the clay platelets are evenly dispersed the distance between plates would be approximately 50 nm. The constrained polymer region would be required to extend at least 25 nm from the surface.

CHAPTER 4

MECHANICAL PROPERTIES OF LAYERED SILICATE THERMOPLASTIC NANOCOMPOSITES

Marlex HGL-350 Polypropylene homopolymer (antistatic) was used as neat resin (density 902Kg/m^3 and melt flow rate 35 g /10 min). The nanoclay used to modify PP matrix was organically modified MMT nanoclay, I.28E, supplied by Nanocor. Permastat 200A Natural Nylon-6 from RTP Company was used as neat resin. The nanoclay used modify Nylon-6 was organically modified MMT nanoclay, I.30T supplied by Nanocor. For pultruded unidirectional composite specimens, E-Glass fibers were pre-impregnated with polypropylene with and without nanoclay (layered silicates), which were initially melt intercalated, using a single-screw extruder (L/D 12:1) to form pre-impregnated (pre-preg) tapes. E-Glass/PP or nanoclay/E-Glass/PP, pre-preg tapes are then pultruded to yield unidirectional composites. Subsequently, 2.54 cm (1 inch)wide and 1.27 cm (0.5 inch) thick composite beams for different nanoclay content (0%, 1%, 2%, 3%, 4%, 5% and 10% by weight) were pultruded. Pultruded E-Glass/PP specimens with different nanoclay loading are shown in Figure 4.1.

E-Glass/Nylon-6 panels of 0.508 cm (0.20 inch) thickness with different weight addition of nanoclay (0%, 4% and 8%) were manufactured by compression molding. Further, test coupons of 15.24 cm (6 inch) in length, 1.27 cm (0.5 inch) in width and a gage length of 2.54 cm (1 inch) were used for compression tests. Short beam shear tests were performed on specimens with dimensions: length 3.048 cm (1.2 inch) width of 1.016 cm (0.40 inch) and a span of 1.778 cm (0.70 inch).

4.1 Manufacturing of E-Glass/PP Nanocomposites by Pultrusion Process

Pultrusion is among the most rapid and efficient processes to fabricate composites when low-cost and/or high volume is required, Liskey (1989), Carsson and Astrom (1998). The process consists of the following general steps: (i) feeding of pre-preg tapes (the pre-impregnation of fibers is usually done in a separate step using an extruder); (ii) die shaping/curing; (iii) pulling station; and (iv) cutting station. The pre-preg tapes (continuous fibers, mats, etc.) are guided through carding plates and other style guides to assemble them in the right place and order. The pre-preg tape is pulled through a pre-former die, which has three heating zones before it reaches the consolidation die. This enables the pre-heating and melting of pre-preg tapes. The operating parameters (temperature/pull speed) are adjusted so that the composite is properly consolidated at the die exit. The pultruded composite experiences natural cooling and is finally cut using high precision diamond saw. In the case of the novel process utilized by the pultrusion machine at the University of Alabama (UA), the pre-preg is guided through a heated pre-former and then through an ultrasonically activated final consolidation die, as shown in Figure 4.2. The ultrasonic vibrations directed into the pre-heated pre-preg by means of a waveguide helps stimulate the flow of resin in the pre-preg. Pressure is also applied to the pre-preg within the die to consolidate the pre-preg to the chosen profile. The ultrasonic vibration at low power input (maximum power: 50 watts) does

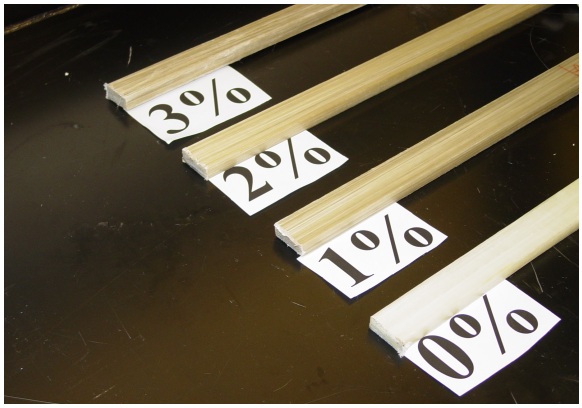

Figure 4.1 Pultruded E-Glass/PP specimens with different nanoclay loadings

result in some incidental heating in the pre-preg, but the increased flow rates of the resin indicates a reduction in viscosity that is far greater than that expected in relation to the temperature increase. The net effect of the ultrasonic die is to reduce effective resin viscosity as well as friction at the composite/die interface, thereby significantly reducing void content and pull-force requirement.

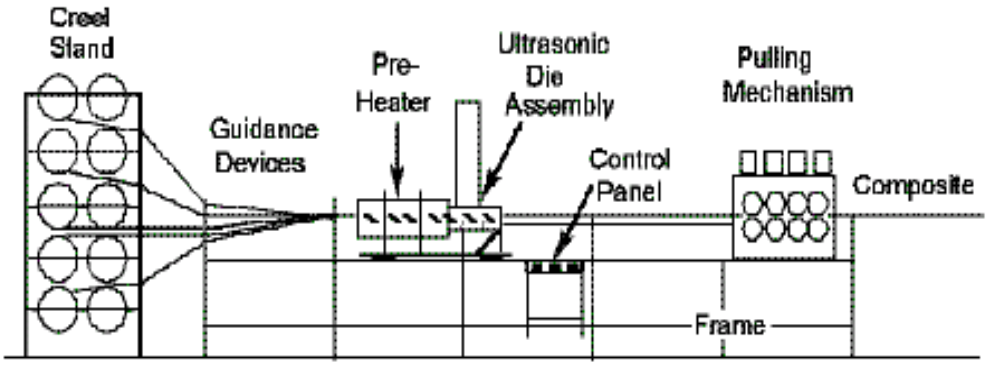

Figure 4.2 Schematic of pultrusion machine with ultrasonic consolidation die

4.2 Manufacturing of E-Glass/Nylon-6 Nanocomposites by Compression Molding

The process requires calculated amount of resin and unidirectional E-Glass fabric to realize the required fiber volume fraction. First, the mold was coated with release spray. Subsequently, calculated amount of Nylon-6 pellets with and without nanoclay was alternated with layers of E-glass fabric in mold. The mold is placed between the heat plates in the hydraulic press, which is water cooled. The hydraulic press, shown in Figure 4.3, is programmed with the desired temperature and pressure cycle for the panel. The E-Glass/Nylon-6 nanocomposite final product is shown in Figure 4.4.

Figure 4.3 Hydraulic press for compression molding

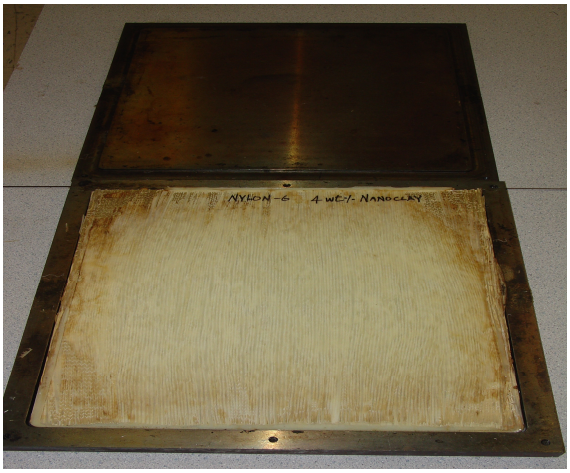

Figure 4.4 Compression molded E-Glass/Nylon-6 nanocomposite panel

4.3. Thermal Analysis

Thermal analysis of pultruded E-Glass/PP based composite and nanocomposites in air were obtained using a TA Instruments 500 Thermo Gravimetric Analyzer (TGA). Dynamic scans from 20 to 800°C (with 20°C per minute heating rate) were conducted. Approximately 10-15 mg specimens of neat resins and nanocomposite were used. The specimen was taken from the mid section of the composite to avoid the skin effect.

The Differential Scanning Calorimetric (DSC) tests were carried out for neat PP and PP nanocomposites with different wt% of nanoclay. TA Instruments 1000 DSC was calibrated with indium standards. The specimens of about 10 mg were sealed in aluminum pans and heated from -70 to 190° C at a scanning rate of 20°C/min under nitrogen atmosphere. The convention for defining the melting point of a polymer is to use the peak temperature of the melt but this value has not been corrected for thermal conductivity.

4.4 Microscopy

4.4.1 Scanning Electron Microscopy (SEM)

The modified nanoclay, Nanomer 1.28E was deposited on a copper tape for SEM characterization. The pultruded E-Glass/PP composite with 3 wt % addition was cut using a diamond saw to sections around 2 mm thick or less. The characterization was performed using a Philips XL 30 SEM. The SEM is equipped with an Energy Dispersive X-ray Spectrometer (EDX) and has both back-scattered electron and secondary electron detectors for imaging. The SEM is operated through a PC based system.

4.4.2 Transmission Electron Microscopy (TEM)

Ultra thin sections (200 nm) of PP resin with nanoclay were cut using an ultramicrotome (EM ULTRACUT UC6, Leica) equipped with a diamond-knife (Diadome, 45 degree) and the sections were supported on carbon film on copper grids. Film thickness was 200 nm and the TEMs used were a JEOL JEM-2200FS with 200kV resolution and a Hitachi H8000.

For pultruded E-Glass/PP nanocomposite characterization, specimens were cut using an ultrasonic disc cutter. These cylinders were then sliced using a diamond saw to 0.5 mm or less, then ground gently with a 600-grade silicon carbide paper to a thickness of about 200 μm and subsequently dimpled by mechanical polishing. These dimpled discs were then ion-milled and thinned to a thickness of less than 100 nm to allow electron beam transmission. The thin foils so prepared were examined with a 200 KeV TEM (Hitachi H 8000) for characterization of fiber reinforced nanocomposites.

4.5 Mechanical Testing

Compression test were performed for neat PP and fiber reinforced composites and nanocomposites in two different (E-Glass/PP and E-Glass/Nylon-6 resin systems). ASTM D695 procedure was used to determine the compressive properties of PP and nanoclay modified PP resin specimens and E-Glass/PP fiber reinforced composite and nanocomposite load was measured by load cell attached to the top platen. Initially, tests were carried out using

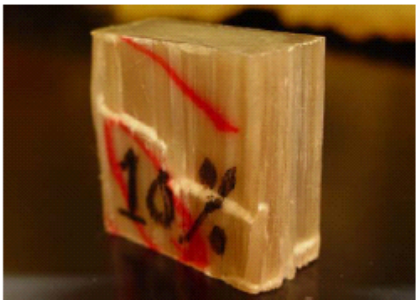

Figure 4.5 Pultruded compression test specimen after failure with 10 wt% nanoclay loading

compression-molded cylindrical test specimens that were 12.7 mm in diameter and 25.4 mm in length. From applied load and displacement data, stress vs. strain curves, were plotted using the Instron fast track data acquisition software. In addition, other mechanical tests, including compression tests (Figure 4.5), short beam shear tests and uni-axial tensile tests, were performed following ASTM standards at an independent testing laboratory for baseline (0 wt % nanoclay) and modified (3 wt %) pultruded PP nanocomposites. Further, compression tests for E-Glass/Nylon-6 composites and nanocomposites were performed according to Illinois Institute of Technology Research Institute (IITRI) standard, as shown in Figure 4.6. Short beam shear test was performed following ASTM D2344, Figure 4.7, and uniaxial tensile test were performed following ASTM D638 for E-Glass/Nylon-6 composites and nanocomposites. At least four replicate test specimens were used per resin per nanoclay loading.

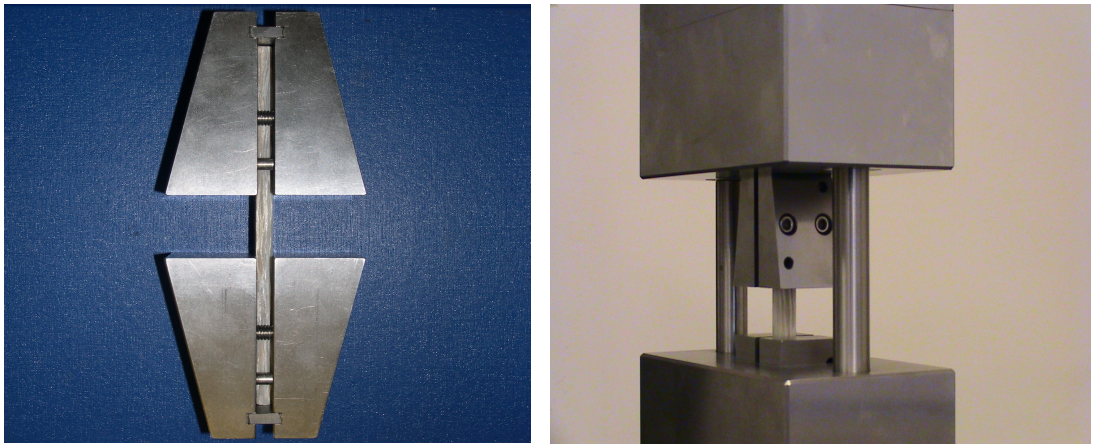

Figure 4.6 IITRI fixtures for compression test

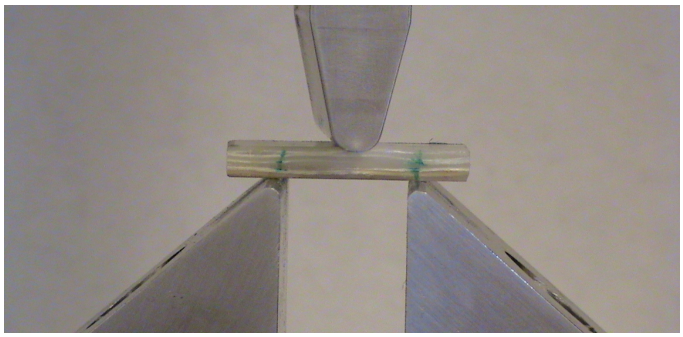

Figure 4.7 Three-point bend fixture for short beam shear test

4.6 Results and Discussion

4.6.1 Thermal Analysis

Thermo gravimetric analysis (TGA) has been done to estimate the thermal stability of conventional fiber reinforced microcomposite and nanocomposite. The PP based nanocomposite decomposes at higher temperature (440°C), as shown in Table 4.1 and Figure 4.8. This improvement in the decomposition temperature (T_{dec}) is attributed to the ability of the silicate layers to retard loss of volatiles and also promote the formation of a char layer, Hussain *et al* (2005) and Shao (2005).

The differential scanning calorimetric studies have been carried out to understand the effect of nanoclay on glass T_g and melt temperature (T_m). Determination of T_g is quite subtle in polypropylene and analysis has been done mainly in neat PP and PP with nanoclay at different wt% of nanoclay in PP resin. Nanocomposite showed negligible effect compare to base polymer (see Figure 4.9).

Table 4.1 T_{dec} of pultruded E-Glass/PP nanocomposites

Nanocomposites	Clay weight %	T_{dec}(°C)
E-Glass/ PP	0%	396.91
	1% nanoclay+PP	427.92
	2% nanoclay+PP	427.23
	3% nanoclay+PP	425.03
	4% nanoclay+PP	426.33
	5% nanoclay+PP	428.27
	10% nanoclay+PP	421.17

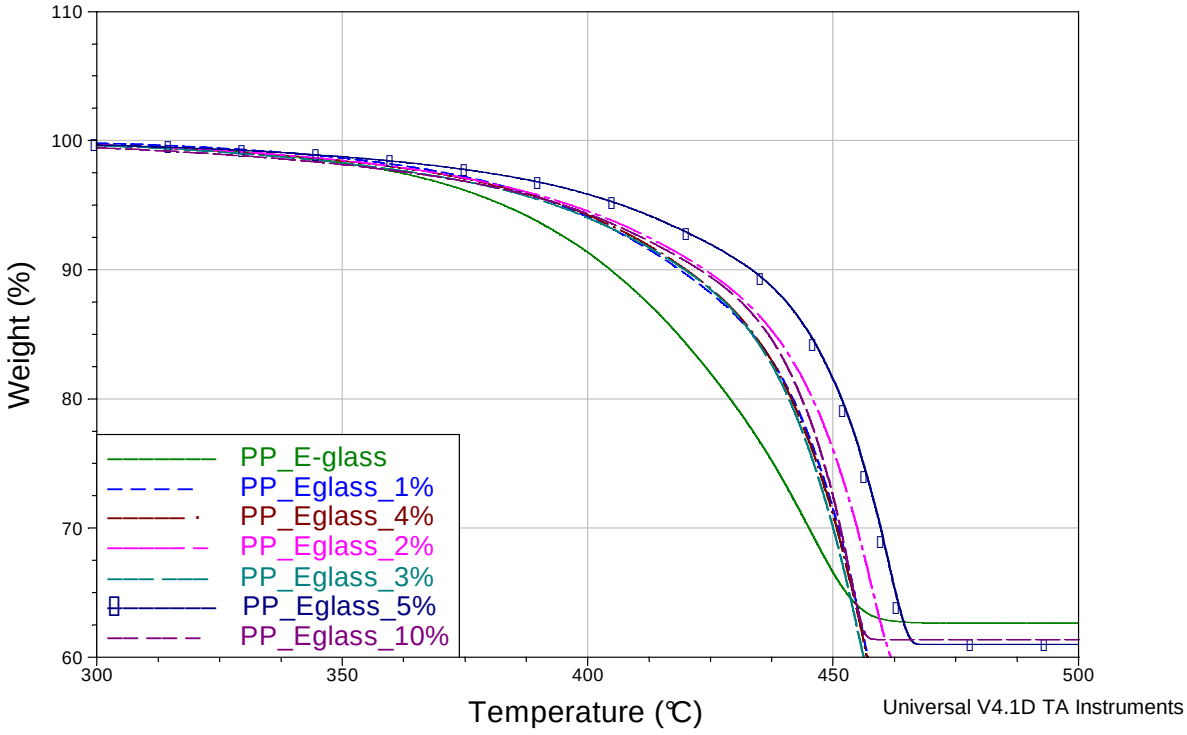

Figure 4.8 TGA thermograms of weight loss versus temperature for pultruded E-Glass/PP Nanocomposites

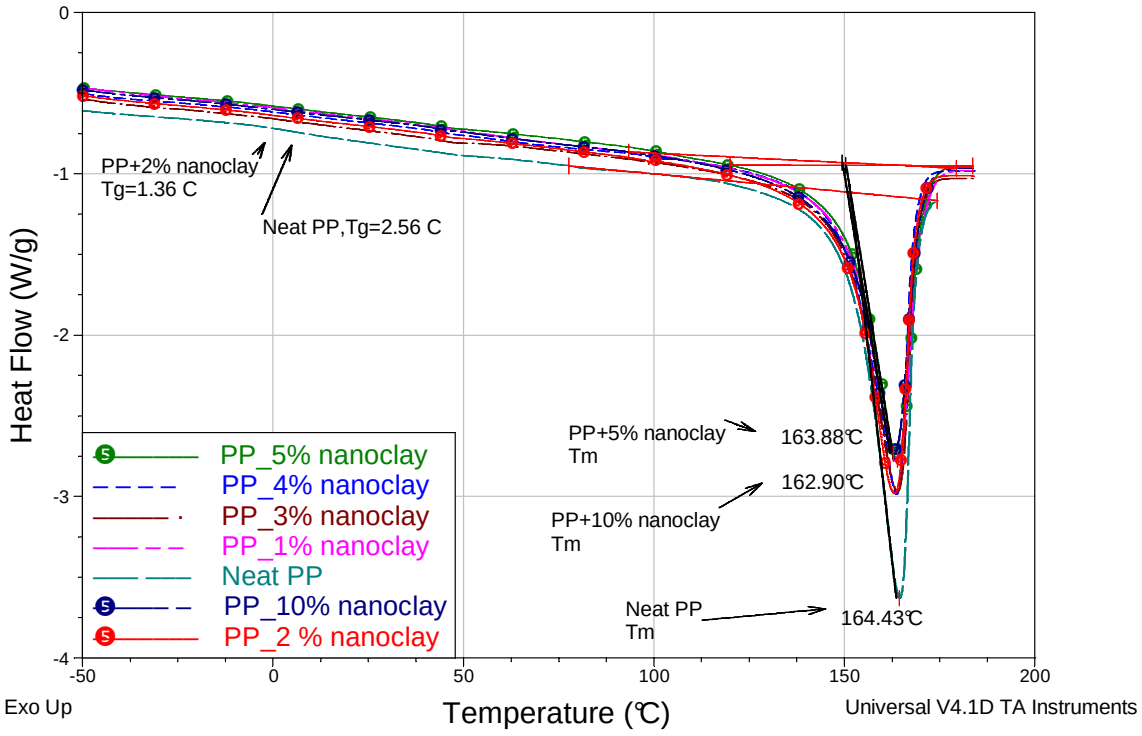

Figure 4.9 DSC curves of neat PP and different nanocomposites

4.6.2 Scanning Electron Microscopy (SEM)

Characterization using SEM with Energy Dispersive X-ray Spectrometer (EDX) was carried out to ascertain the chemical constituents of nanoclay and the pultruded composite. Nanomer I.28E obtained from Nanocor is surfactant modified MMT nanoclay. The nanoclay is modified using octadecylamine (ODA) as surfactant. First, nanoclay was characterized using SEM with EDX as shown in Figures 4.10(a) & (b). The EDX pattern for a complete scan indicated presence of Aluminum, Silica, Oxygen, Magnesium and Carbon (due to the surfactant ODA modification). These compositions compare well the Chemical Analysis from Nanocor shown in Table 4.2.

Further the pultruded E-Glass/PP composite with 3 wt% nanoclay was characterized using SEM with EDX (Figures 4.11(a) &(b)). The EDX patterns for a complete scan at 50μm revealed a

strong presence of calcium and carbon along with aluminum, silica oxygen and magnesium. The strong presence of carbon is due to the PP matrix. An EDX pattern, Figure 4.12(b) obtained for a local scan indicated in Figure 4.12(a) showed presence of potassium and sodium in addition to the chemical constituents for a complete scan. The peaks of sodium and potassium indicate the presence of nanoclay when compared with the chemical analysis shown in Table 4.3. To validate the presence of calcium a local scan indicated in Figure 4.13(a) on glass fiber revealed an EDX pattern, Figure 4.13(b), with presence of aluminum, silica, oxygen and calcium without presence of carbon. The pattern obtained compared well with the composition of E-glass fiber, shown in Table 4.3.

Table 4.2 Chemical analysis for unmodified Nanomer I.28E
(Courtesy Nanocor)

Element	**Polymer Grade MMT (weight %)**
O	48.35
Na	4.76
Mg	2.36
Al	12.32
Si	29.3
P	0.01
S	0.13
K	0.18
Ca	0.21
Ti	0.11
Mn	0.02
Fe	2.25
TOTAL	100.00

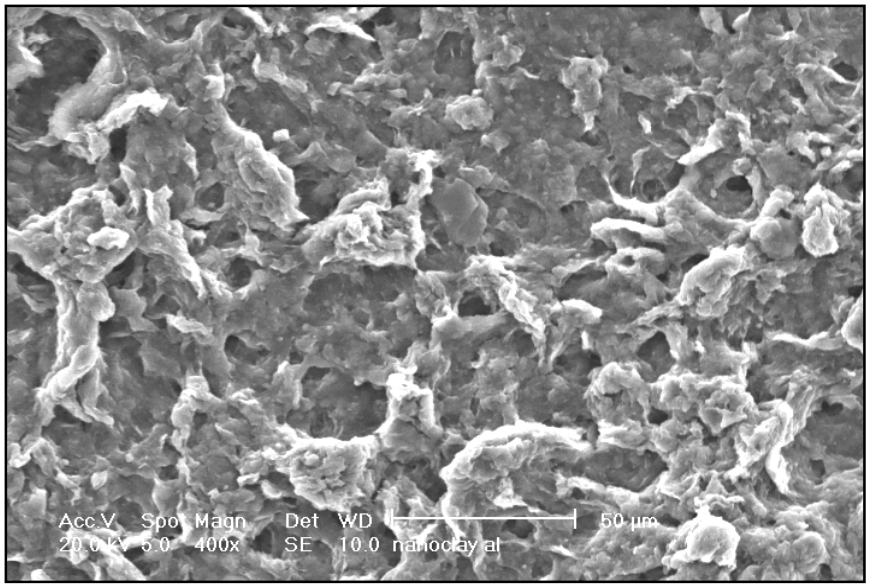

Figure 4.10(a) SEM image for modified nanoclay, Nanomer I.28E

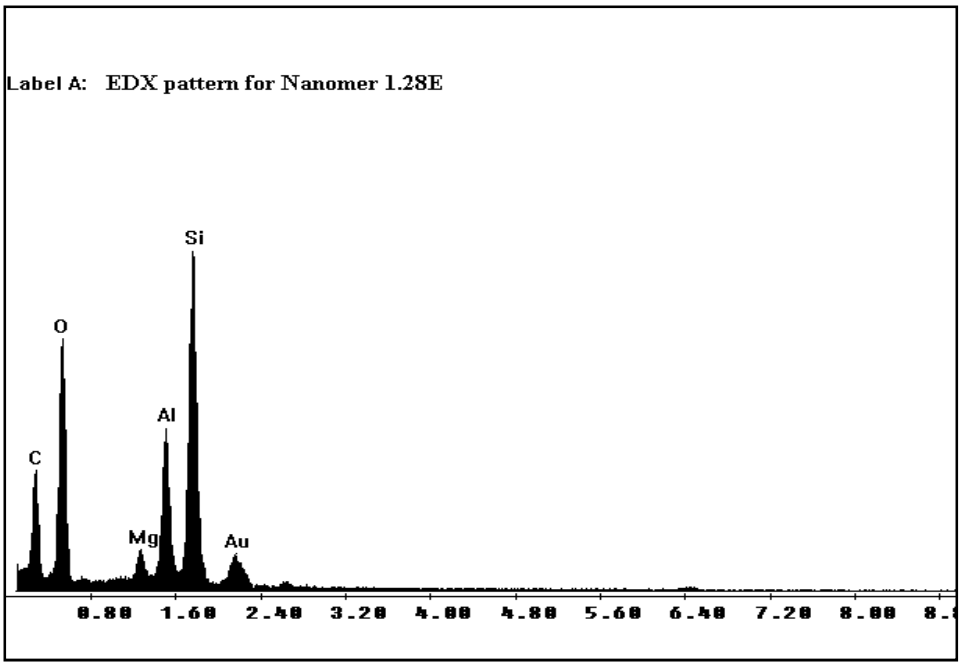

Figure 4.10(b) EDX pattern for modified nanoclay, Nanomer 1.28E

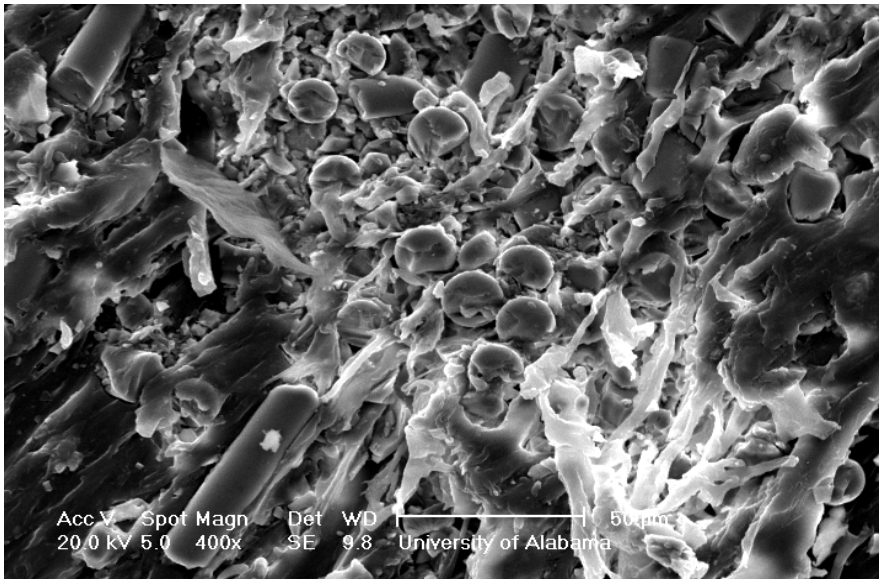

Figure 4.11(a) SEM image for pultruded E-Glass/PP composite with 3 wt% nanoclay

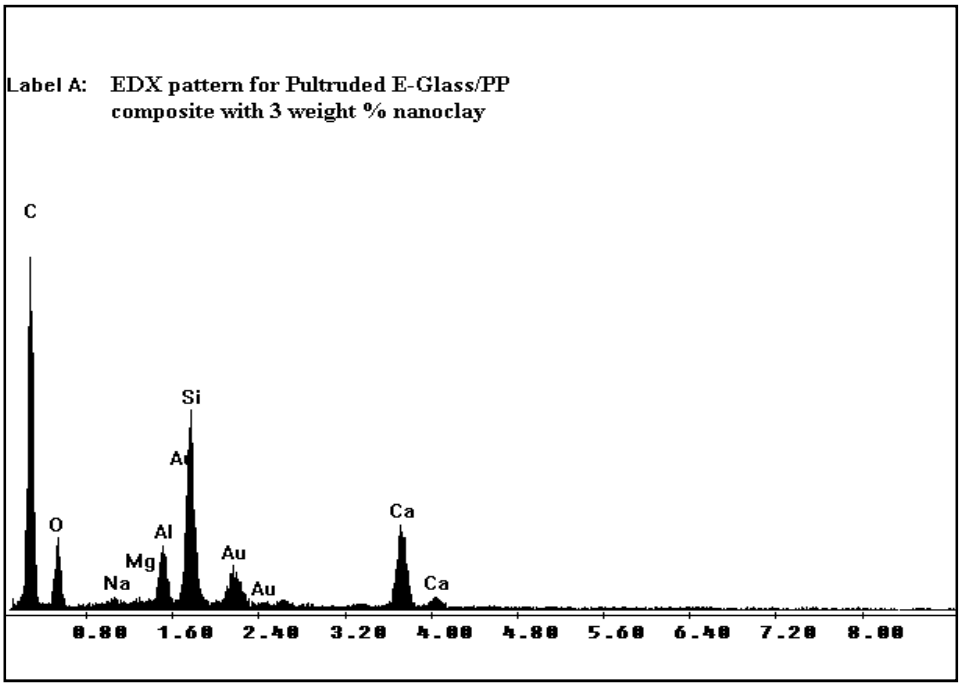

Figure 4.11(b) EDX pattern for E-Glass/PP composite with 3 wt% nanoclay

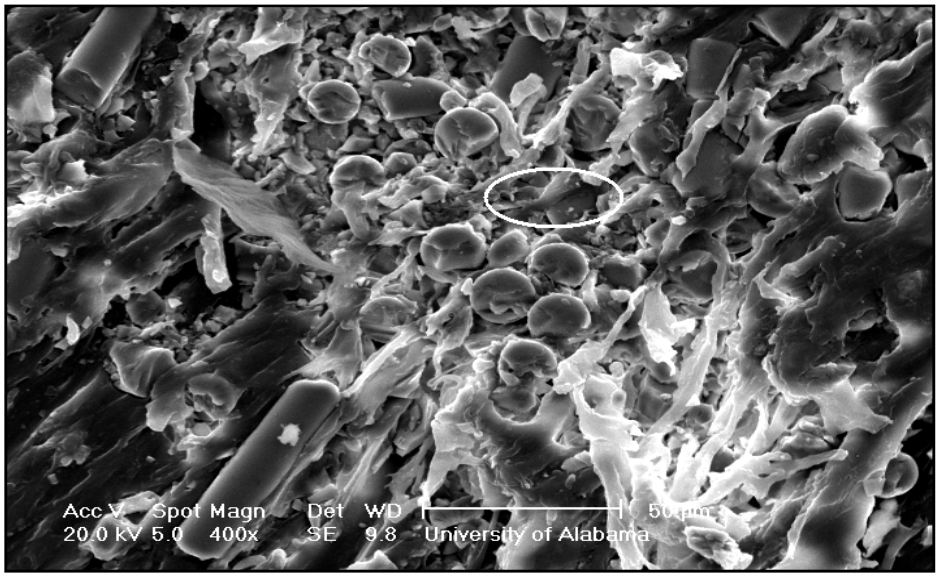

Figure 4.12(a) SEM image for pultruded E-Glass/PP composite with 3 wt% nanoclay (indicating area for interest for EDX)

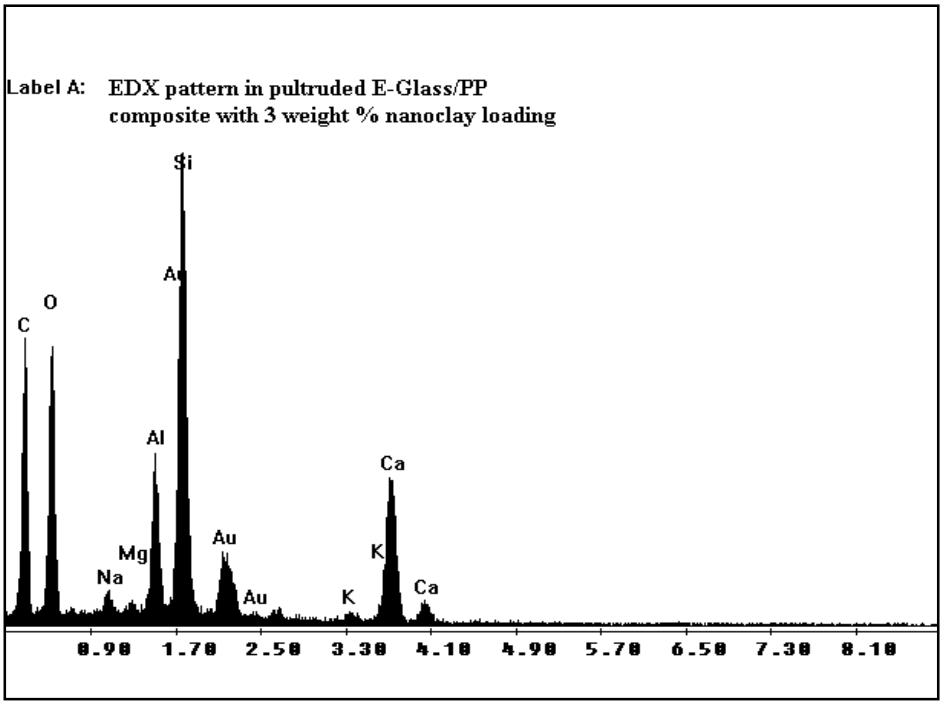

Figure 4.12(b) EDX pattern for local scan in E-Glass/PP composite with 3 wt% nanoclay

Figure 4.13(a) SEM image for indicating glass fiber in pultruded E-Glass/PP composite with 3 wt% nanoclay

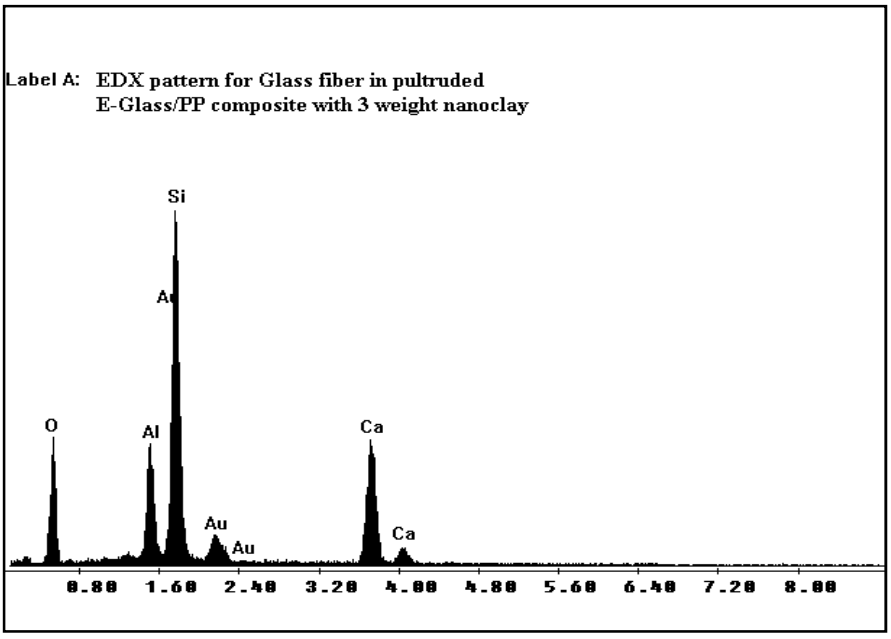

Figure 4.13(b) EDX pattern for Glass fiber in E- Glass/PP composite with 3 wt% nanoclay

Table 4.3 Composition for E-Glass (Courtesy Saint-Gobain Vetrotex)

Composition	**E-Glass (weight%)**
Silica (SiO_2)	53 to 55 %
Alumina (Al_2O_3)	14 to 15.5%
Calcium Oxide (CaO)+Magnesium Oxide (MgO)	20 to 24 %
Boron oxide (B_2O_3)	6.5 to 9 %
F_2	0 to 0.7 %
Miscellaneous	< 2%

4.6.3 Transmission Electron Microscopy (TEM)

To gain insight into the morphology of pultruded nanocomposites, characterization using TEM was conducted at lower and higher magnification for 5 wt% and 10 wt% clay based PP nanocomposite specimens, as shown in Figure 4.14 and Figure 4.15**.** Nanocomposites containing 5 wt% and 10 wt% of nanoclay show heterogeneous dispersion, presence of aggregates, as well as resin rich areas in the matrix without clay. However, there are regions where completely delaminated sheets are dispersed individually, showing as dark lines of 10-Å thickness. It appears that the clay exists as expanded aggregates made up of 5 to 12 platelets. The size of these aggregates and the number of platelets in them increase with the percentage of clay within the PP matrix. However, it is of interest to mention that the degree of intercalation or exfoliation depends on the type of clay and its surface modification. It is also important to mention that the

process condition has a strong effect on delaminations and dispersion of clay platelets. Moreover extruder type (whether it is single or multi-screw) and screw configurations play an important role in delamination of clay agglomerates, Paul (2001) and Wu and Zhang (2002). Basically melt intercalation involves the mixing of clay with molten polymer. Homogenous dispersion of layered silicates is very difficult as the nanoclay has strong tendency to agglomerate and PP is a highly viscous material. In Figure 4.14(b-c), the average distance between clay platelets and the average length of the platelets for a 5 wt% clay nanocomposite are 3.5 and 200 nm, respectively. Similarly, in Figure 4.15(b-c), the average distance between clay platelets and the average length of the platelets for a 10 wt% clay nanocomposite are 3 nm and 200 nm, respectively. Consequently the final structure achieved in this process is intercalated morphology. It has also been observed that the processing of nanocomposite using extruder and preparation of the specimens using injection molding reduces the initial aspect ratio of clay platelets from 1000 to 180-220. However, the resultant nanocomposites still exhibit significant improvement of mechanical and thermal properties as discussed later. In Figures 4.14(c) and 4.15(c) it should be noted that the interlayer spacing (gallery spacing) is expanded; the layer-layer distance is about 25nm.

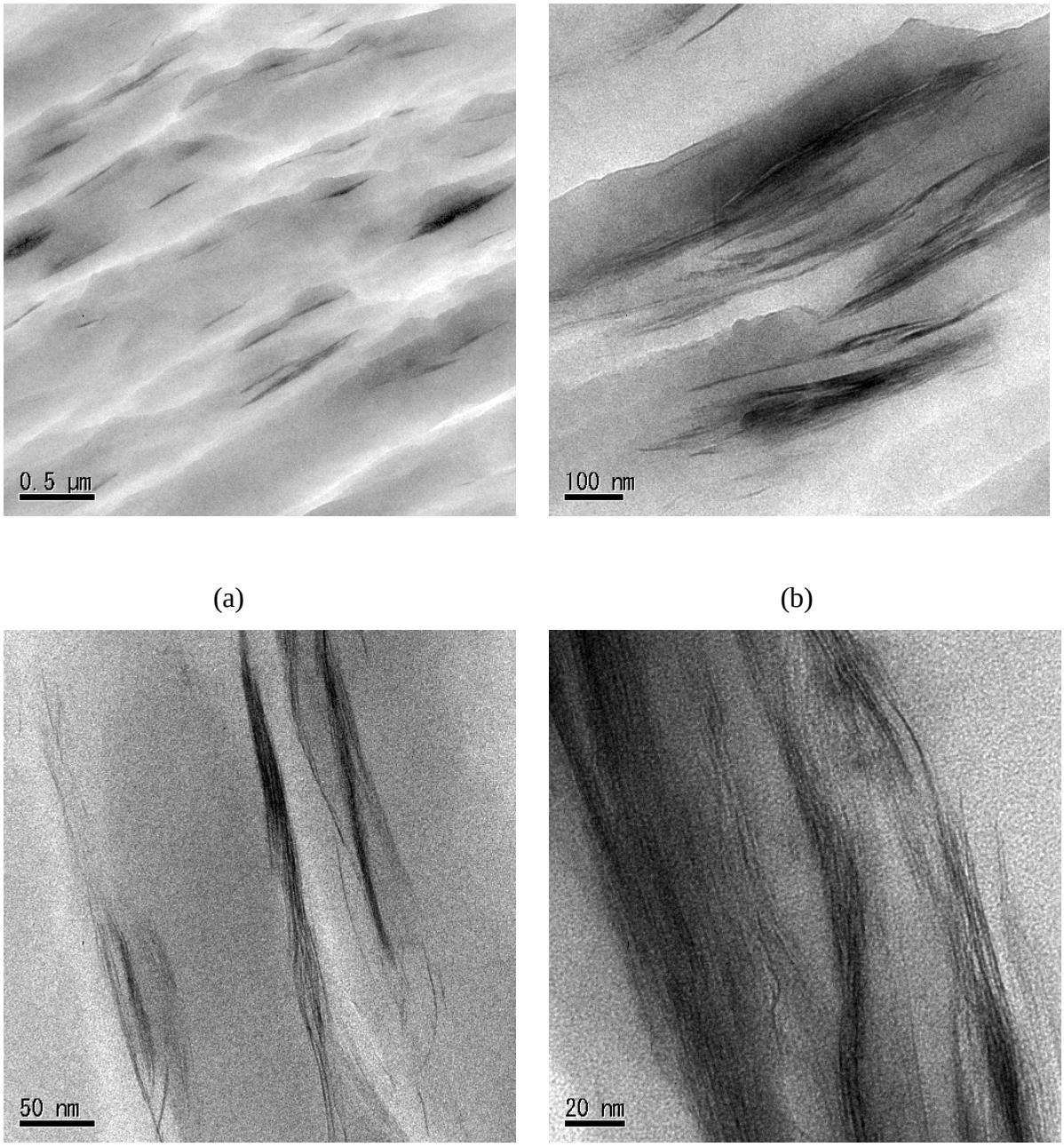

(a) (b)

(c) (d)

Figure 4.14 TEM micrograph of PP with 5 wt% clay loading at different magnifications

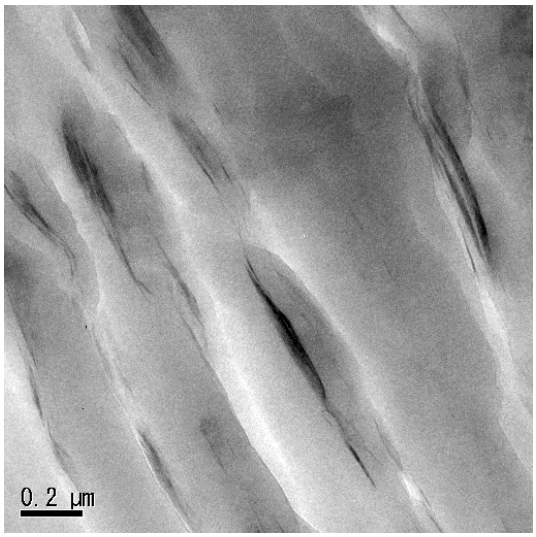

(a)

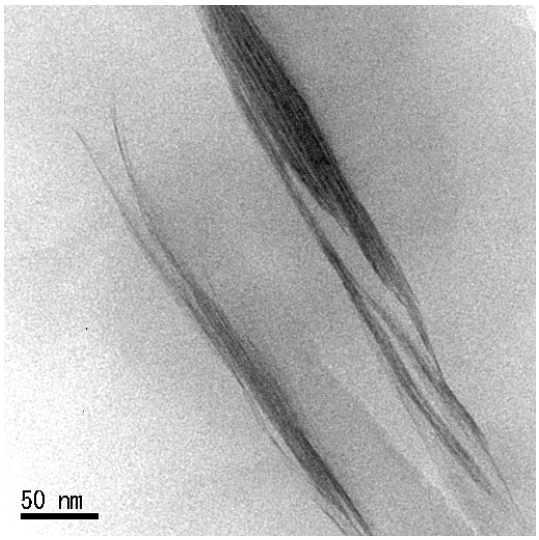

(b)

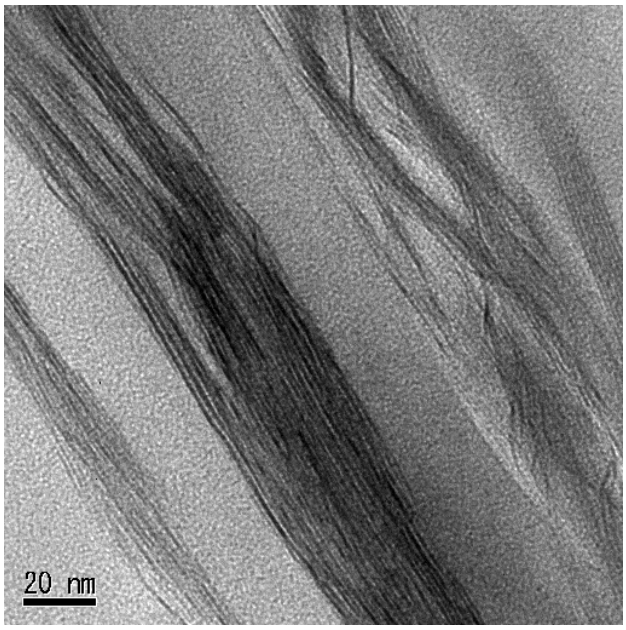

(c)

Figure 4.15 TEM micrograph of PP with 10 wt% clay loading at different magnifications

4.6.4 Mechanical Testing of E-Glass/PP Nanocomposites

Compression test

In order to characterize the effect of nanoclay on the compressive properties of neat resin, cylindrical specimens of PP were compression molded as shown in Figure 4.16. Compression strength data for neat polypropylene (PP) resin for different nanoclay loading are tabulated in Table 4.4. The bar chart in Figure 4.17 shows the progressive improvement in the normalized compressive strength of nanoclay reinforced PP for different nanoclay content. A 134% increase in compressive strength is observed for PP resin with 10 wt% nanoclay loading. Stress verses strain curves for nanoclay reinforced E-Glass/PP composite are shown in Figure 4.18 for different nanoclay loadings, and the compressive strength data are summarized in Table 4.5. The bar chart in Figure 4.19 shows the monotonic improvement in the normalized compressive strength of pultruded E-Glass/PP composite with different nanoclay content. Each bar represents the average of four test specimens, with a standard deviation of roughly 5 %. A 122 % improvement in compressive strength for 10 wt% nanoclay content is observed as compared with baseline E-Glass/PP specimens with zero nanoclay content. A similar dramatic enhancement is measured for normalized compressive modulus (stiffness) as shown in Figure 4.20, where 10 wt% clay reinforcement results in a 110 % improvement in compressive modulus. From these charts it is apparent that a significant improvement in compressive strength (87%) as well as modulus (99%) is attainable for E-Glass/PP system even with only 5 wt% nanoclay content while using purely mechanical (un-optimized) means of nanoclay dispersion, namely, a single-screw extruder and sonication at the die. Examination of TEM micrographs of pultruded specimens indicate presence of intercalated morphology with heterogeneous dispersion, which, when fully exfoliated would presumably yield even better mechanical properties. Any negative

effect of the ultrasonic treatment on fiber alignment is small compared with the large increase in matrix strength due to the presence of nanoclay particles. Further, the test data indicate that it is feasible to pultrude nanoclay reinforced E-Glass/ PP laminates with up to 27% fiber volume fraction and up to 10 wt% nanoclay content without a deleterious increase in resin viscosity that could potentially clog the consolidation die and/or result in poor wetting of the fibers, Roy *et al* (2007).

Figure 4.16 Cylindrical Specimen with 3 wt% nanoclay loading in neat PP

Table 4.4 Compression test data for neat PP resin and nanoclay modified resin

Specimen	Clay (wt%)	Avg. Compressive strength (MPa)	% Increase Compressive strength
PP	0.0	6.51	-
PP	1.0	8.29	26
PP	2.0	9.42	42
PP	3.0	10.33	57
PP	4.0	11.01	67
PP	5.0	12.77	94
PP	10.0	15.37	134

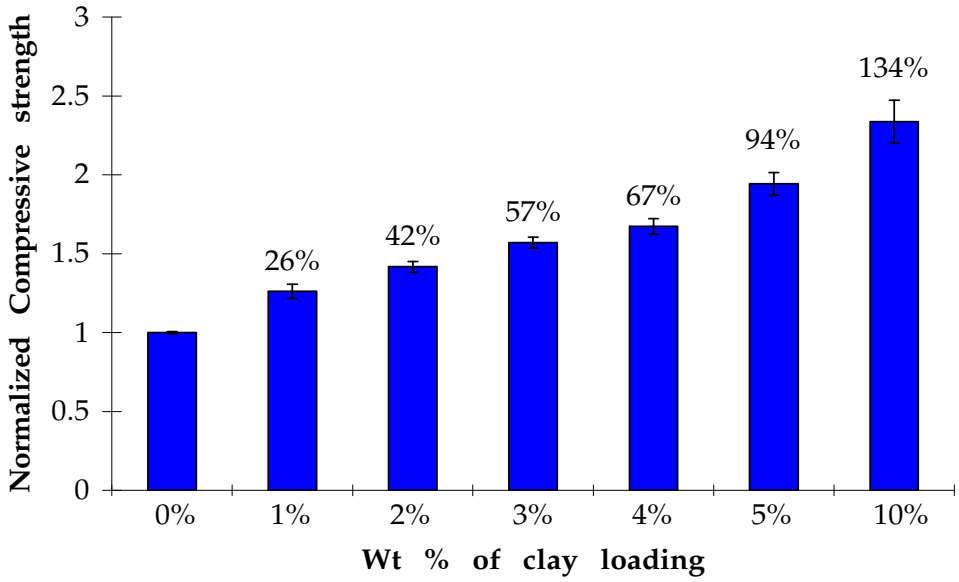

Figure 4.17 Normalized compressive strength versus clay content for neat PP

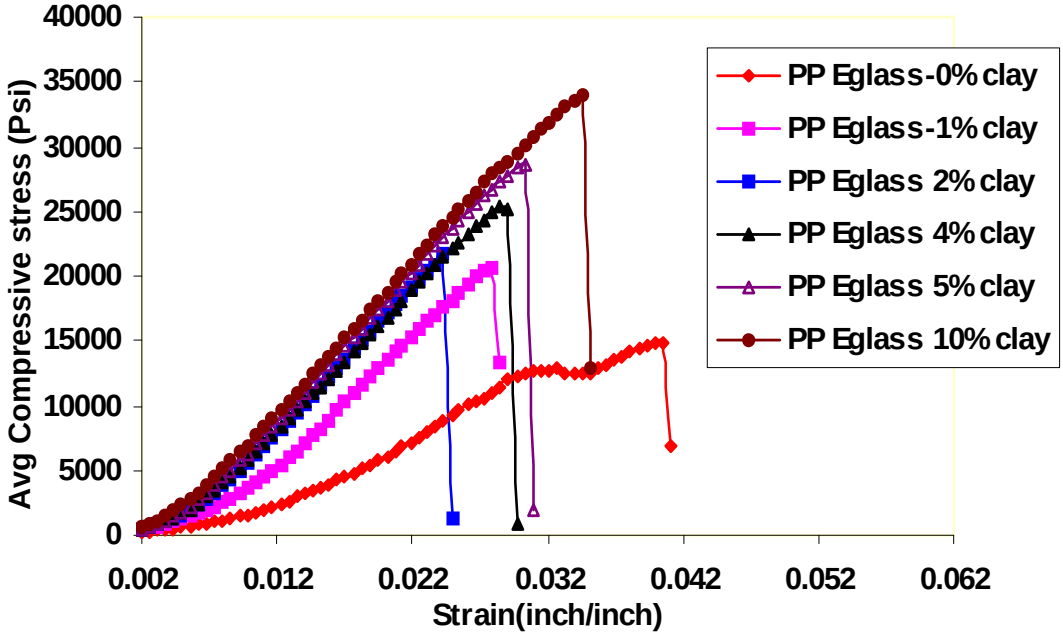

Figure 4.18 Comparison of stress versus strain curves from compression test for pultruded E-Glass/PP nanocomposite with different nanoclay loadings

Table 4.5 Compression test data for E-Glass/PP pultruded composites

Specimen	Clay (wt%)	Avg. Compressive strength (MPa)	Avg. Compressive modulus (GPa)	% Increase	
				Strength	Modulus
E-Glass/PP	0.0	105.32	4.12	-	
E-Glass/PP	1.0	139.78	6.68	32.72	61.86
E-Glass/PP	2.0	146.51	6.97	39.11	69.06
E-Glass/PP	3.0	155.57	7.10	47.72	72.31
E-Glass/PP	4.0	175.59	7.92	66.73	92.02
E-Glass/PP	5.0	197.31	8.23	87.35	99.66
E-Glass/PP	10.0	233.97	8.67	123.93	110.19

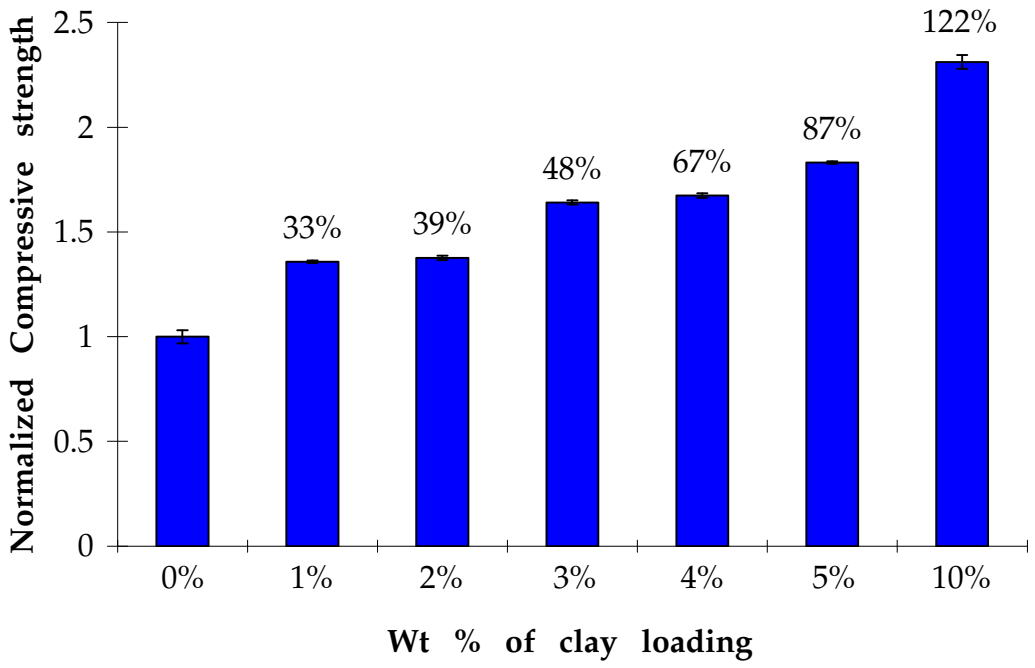

Figure 4.19 Normalized compressive strength versus clay content for pultruded E-Glass/PP nanocomposite

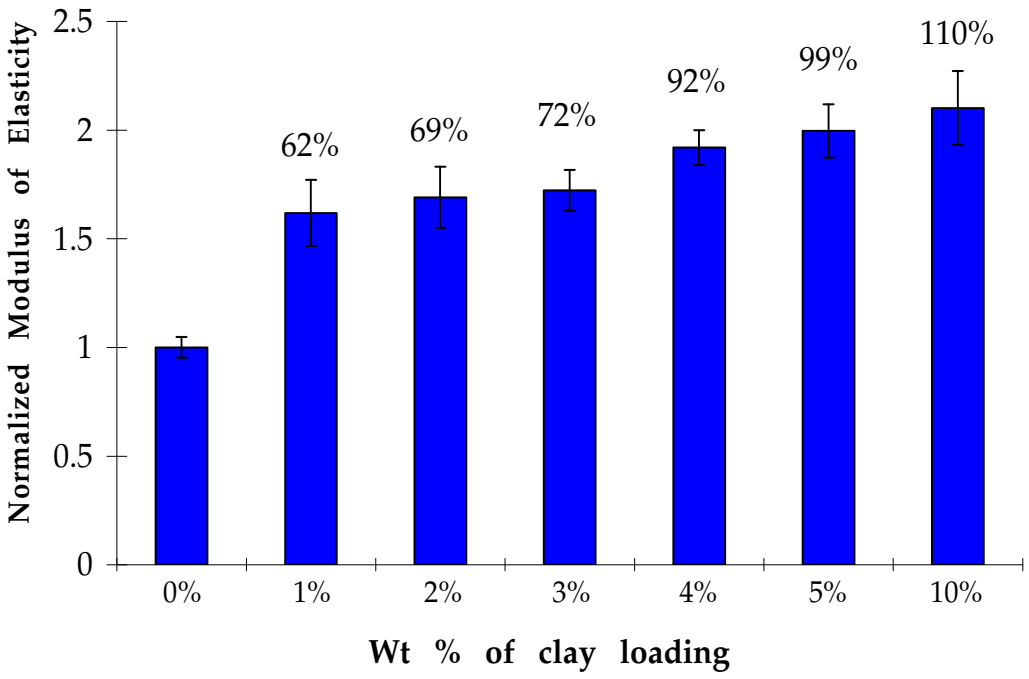

Figure 4.20 Normalized compressive modulus versus clay content for pultruded E-Glass/PP nanocomposite

4.6.5 Mechanical properties of Nanocomposite tested at Independent Test Laboratory

The objective was to study the effect on mechanical properties of modified pultruded PP/Glass fiber composite with 3 wt% addition of nanoclay and compare with baseline pultruded PP/Glass fiber composite with 0 wt % addition nanoclay. Compression, short-beam shear and uni-axial tensile tests on pultruded PP/E-glass fiber with nanoclay loading of 3 wt% following ASTM standards were performed at an independent testing laboratory and reported here in the interest of completeness. Three specimens were tested for each case. The compressive strength of modified pultruded PP composite showed a significant increase (~110%) as shown in Figure 4.21, which corroborates compressive test data presented earlier in Figure 4.19. The short beam shear tests showed a substantial increase in shear strength (~60%) with modified pultruded PP composite, shown in Figure 4.22. Uniaxial tensile tests to determine tensile strength showed a small increase

of 3.4% (Figure 4.23**)** for modified pultruded PP composite with nanoclay loading of 3wt%. Hence the improvement in compressive and shear properties did not occur at the expense of lower tensile strength of the modified pultruded PP composite, as validated by tensile tests. The normalized mechanical properties data from the independent test laboratory are summarized in Table 4.6.

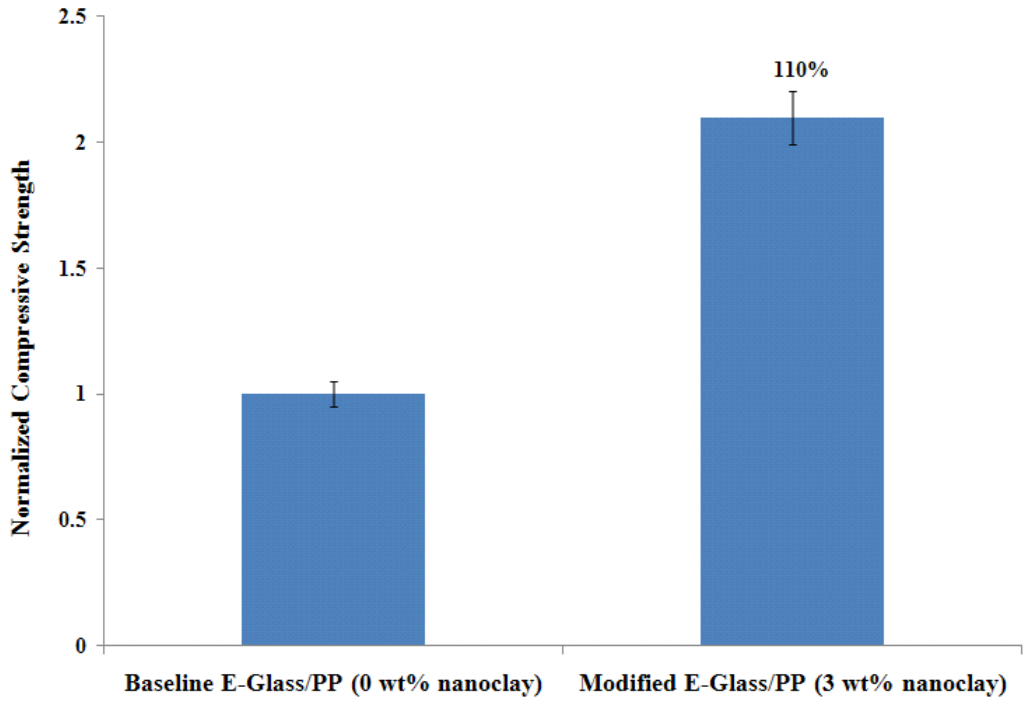

Figure 4.21 Normalized compressive strength comparison for baseline and modified pultruded E-Glass/PP nanocomposite

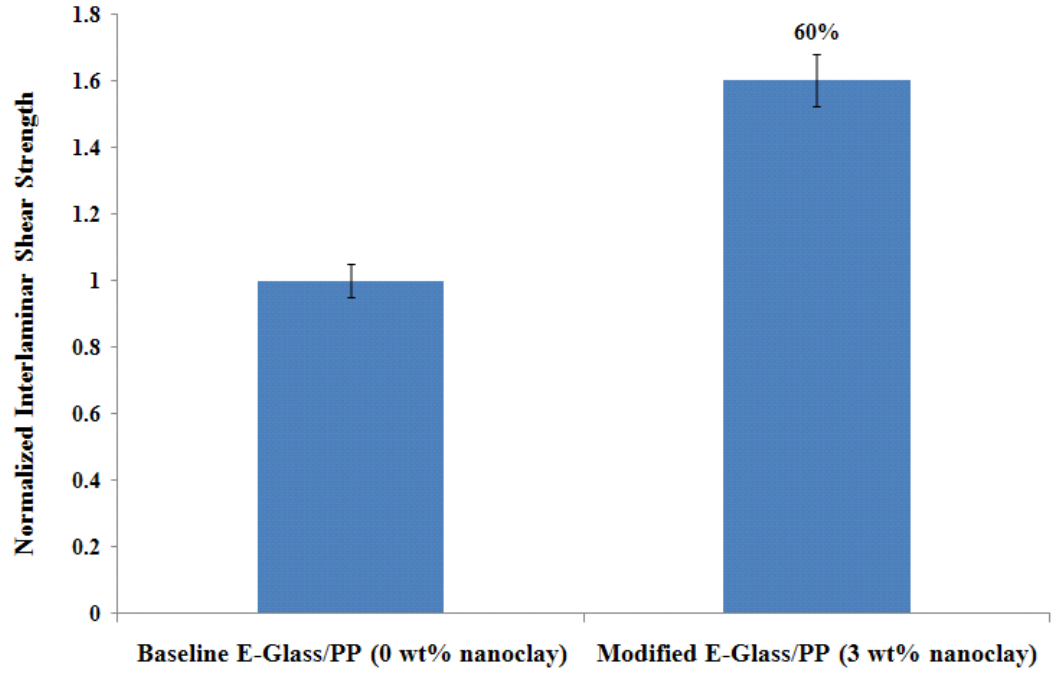

Figure 4.22 Normalized short beam shear strength comparison for baseline and modified pultruded E-Glass/PP nanocomposite

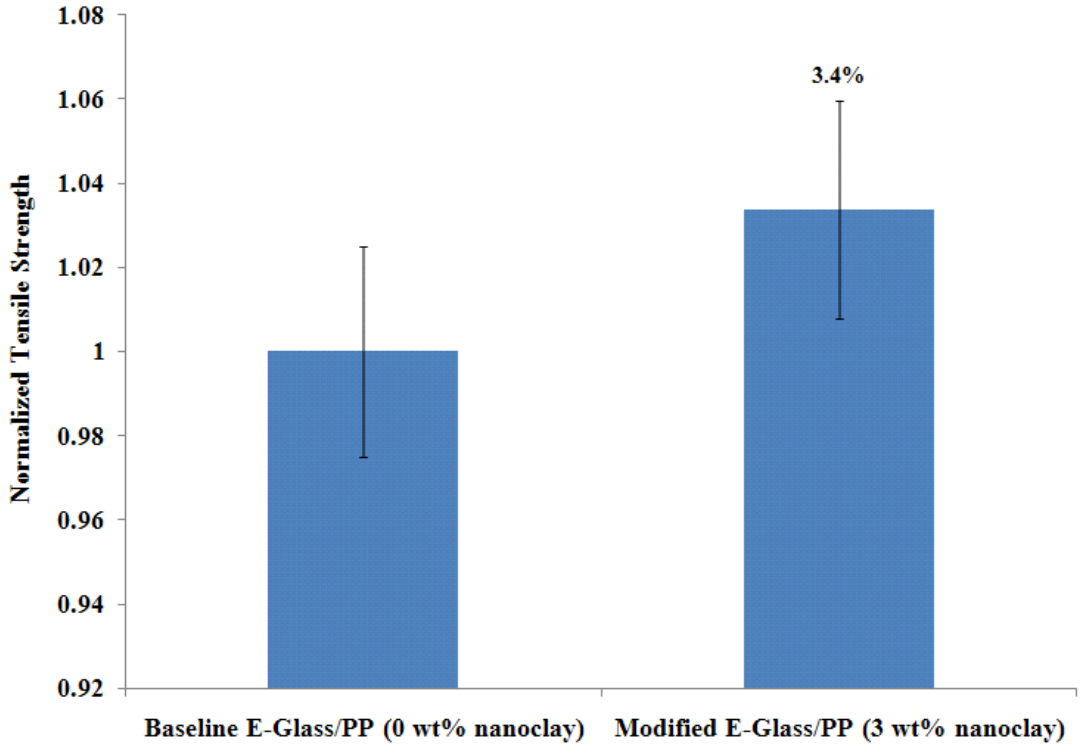

Figure 4.23 Normalized tensile strength comparison for baseline and modified pultruded E-Glass/PP nanocomposite

Table 4.6 Comparison of mechanical properties for pultruded E-Glass/PP composites

Averaged Mechanical Properties at room temperature	Baseline Pultruded E-Glass/PP (Baseline)	Modified Pultruded E-Glass/PP (3% nanoclay)
Normalized Compressive Strength	1	2.10
Normalized short beam shear strength	1	1.60
Normalized Tensile Strength	1	1.03

4.6.6 Mechanical Properties of E-Glass/Nylon-6 Nanocomposites

Compression test

E-Glass/Nylon-6 specimens with different weight addition nanoclay loading were characterized in compression to study the effect of nanoclay. The results (Table 4.7) showed significant improvement in compressive strength with addition of nanoclay, with a peak improvement (~50%) at 4 wt% nanoclay loading and (~34 %) at 8 wt% nanoclay loading, as shown in the bar chart in Figure 4.24. However, unlike the E-Glass/PP nanocomposite, E-Glass/ Nylon-6 exhibits optimum improvement in compressive strength at 4 wt% nanoclay, followed by a decline in reinforcement effectiveness at higher clay loadings. The compressive modulus of E-Glass/Nylon-6 specimens also showed a similar trend with a peak improvement (~24%) at 4 wt% nanoclay loading and (~19 %) at 8 wt% nanoclay loading, as shown in the bar chart in Figure 4.25.

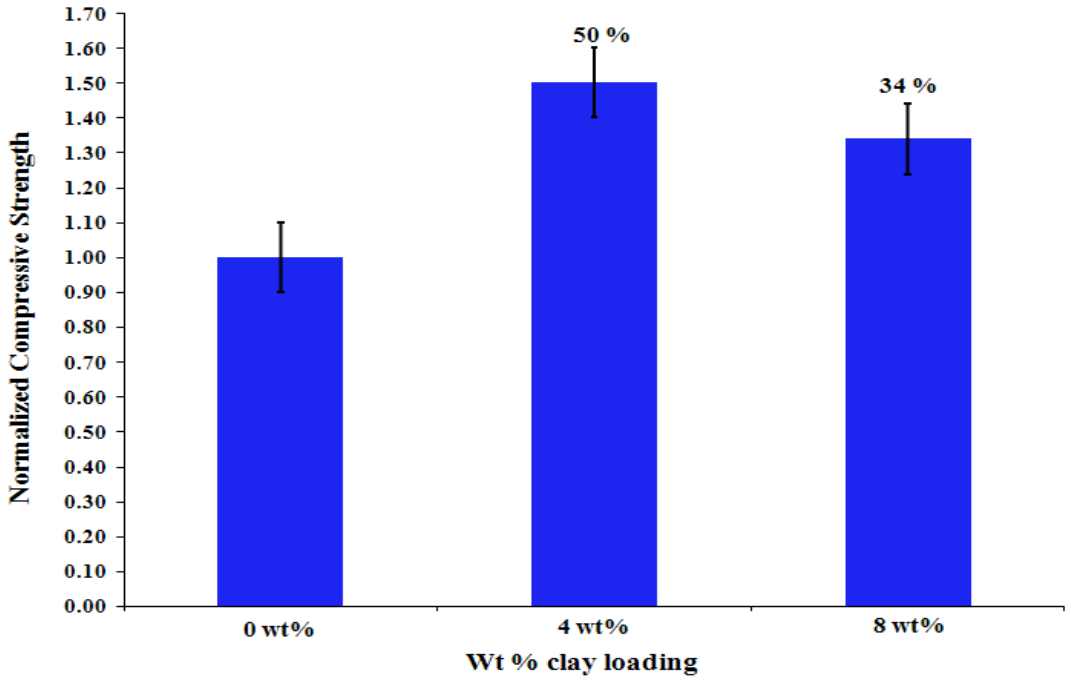

Figure 4.24 Normalized compressive strength versus clay content comparison for E-Glass/Nylon-6 nanocomposite

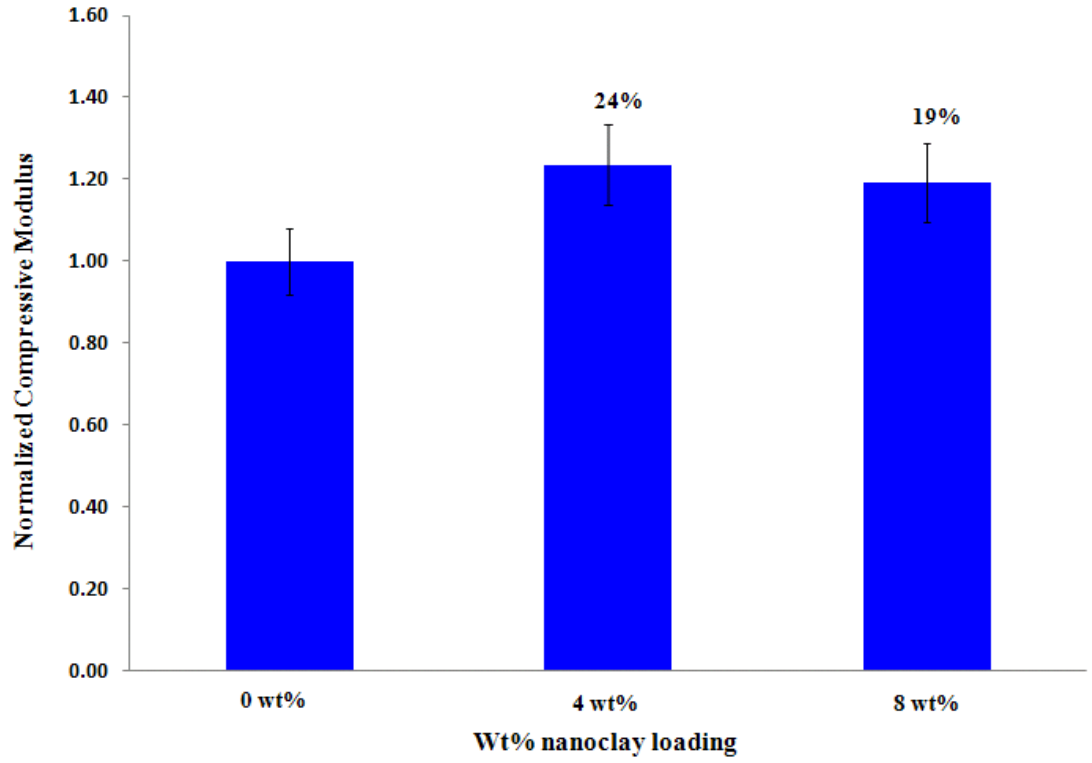

Figure 4.25 Normalized compressive modulus vs. clay content comparison for E-Glass/Nylon-6 nanocomposite

Table 4.7 Compression test data for E-Glass/Nylon-6 composites

Specimen	Clay (wt%)	Avg. Compressive strength (MPa)	% Increase Compressive strength
E-Glass/Nylon-6	0	112.44	-
E-Glass/Nylon-6	4	168.83	50.16
E-Glass/Nylon-6	8	150.59	33.94

Short Beam Shear test

In order to evaluate the effect of nanoclay on interlaminar shear strength of E-Glass/Nylon-6, short beam shear tests were performed. The test results (Table 4.8) indicated a peak interlaminar shear strength improvement of 36.3 % with 4 wt% nanoclay and 3.2% with 8 wt% nanoclay, as shown in Figure 4.26. However, unlike the E-Glass/PP nanocomposite, E-Glass/ Nylon-6 exhibits optimum improvement in compressive strength at 4 wt% nanoclay, followed by a decline in reinforcement effectiveness at higher clay loadings.

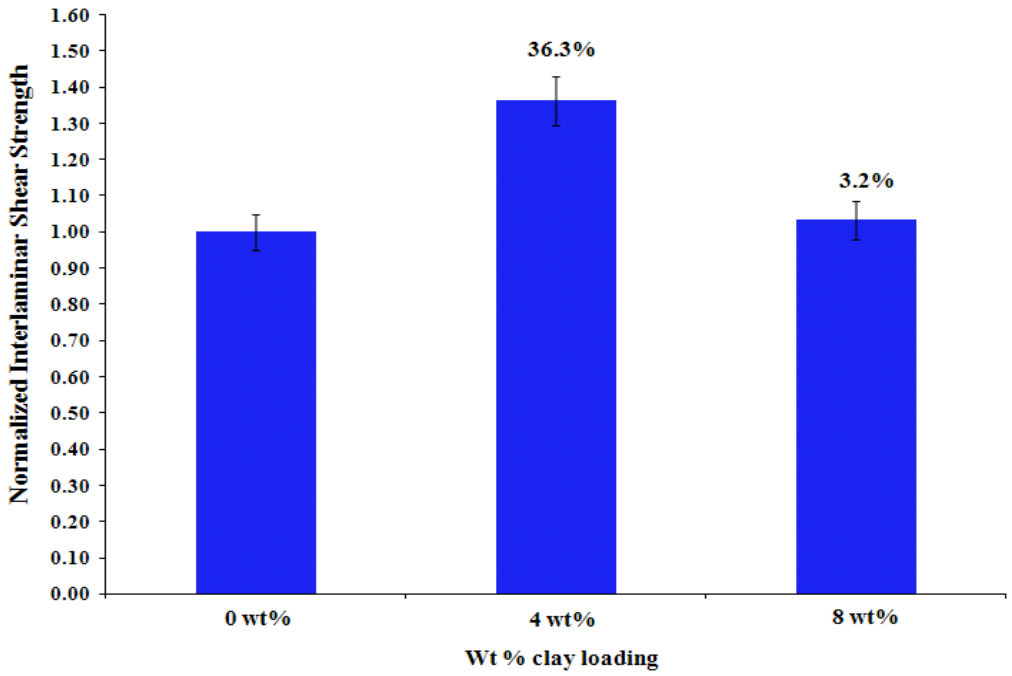

Figure 4.26 Normalized short beam shear strength versus clay content comparison for E-Glass/Nylon-6 nanocomposite

Table 4.8 Short beam shear test data for E-Glass/Nylon-6 composites

Specimen	Clay (wt%)	Avg. Interlaminar shear strength (MPa)	% Increase Interlaminar shear strength
E-Glass/Nylon-6	0	21.39	-
E-Glass/Nylon-6	4	29.15	36.31
E-Glass/Nylon-6	8	22.08	3.24

The normalized mechanical property data for E-Glass/Nylon-6 nanocomposites is summarized in Table 9.

Table 4.9 Comparison of mechanical properties for E-Glass/Nylon-6 composites

Averaged Mechanical Properties at room temperature	E-Glass/Nylon-6 (0 wt % nanoclay)	E-Glass/Nylon-6 (4 wt % nanoclay)	E-Glass/Nylon-6 (8 wt % nanoclay)
Normalized Compressive Strength	1	1.50	1.34
Normalized Short Beam Shear Strength	1	1.36	1.03

Tensile test

Although the primary objective for using nanoclay is to enhance matrix dominated properties, E-Glass/Nylon-6 tensile coupons fabricated were characterized in tension to investigate any detrimental effects due to nanoclay on tensile properties. The tensile tests showed a slight improvement of 3.2% in tensile strength with 4 wt% nanoclay addition, as shown in Figure 4.27.

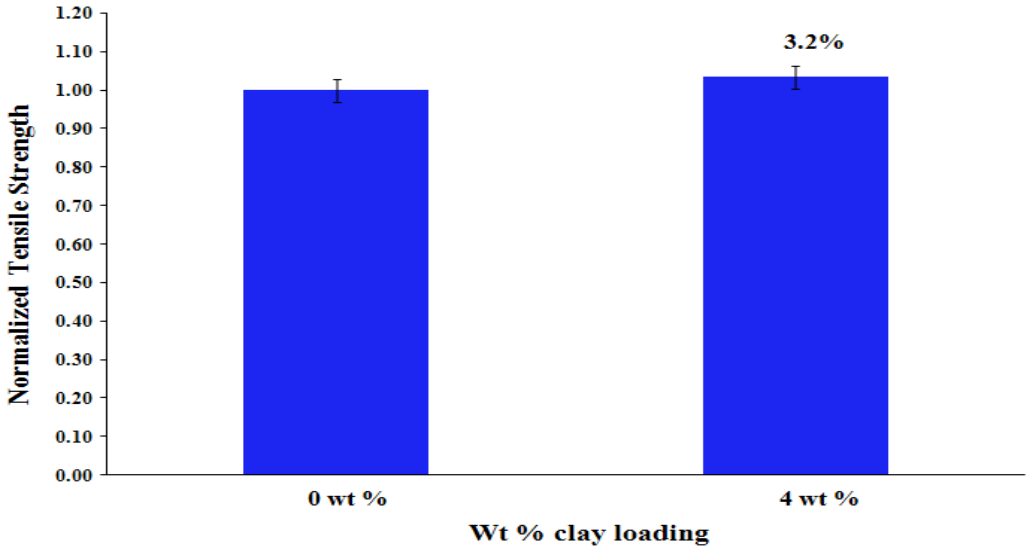

Figure 4.27 Normalized tensile strength versus clay content for E-Glass/Nylon-6 nanocomposite

CHAPTER 5

MOISTURE BARRIER PROPERTIES OF SILICATE LAYERED THERMOPLASTIC NANOCOMPOSITES

5.1 Hygrothermal ageing

E-Glass fiber reinforced Nylon-6 baseline composites and nanoclay (4 wt%) modified E-Glass fiber reinforced Nylon-6 nanocomposites were hygrothermally aged. The specimens were 6 inches x 0.5 inches x 0.2 inches in dimensions according to IITRI standards. The specimens were completely immersed in de-ionized water and placed in an environmental chamber at 50°C. The specimens were weighed at regular intervals and a replicate of 6 specimens were used and the average moisture uptake (M_t) was followed as a function of square root of time until the equilibrium (M_∞) was reached.

The moisture uptake chart is shown in Figure 5.1. The diffusivity of 4 wt% nanoclay loading is halved, as seen in Table 5.1, showing improved barrier resistance. The saturation moisture uptake for nanoclay (4 wt%) modified E-Glass fiber reinforced nylon6 was significantly reduced (~30%) compared to moisture uptake compared to baseline E-Glass fiber reinforced Nylon-6. Moisture diffusion followed Fickian diffusion and the curve fit using Ficks law is shown in Figure 5.2 for baseline E-Glass/Nylon-6 composite and for nanoclay modified E-Glass/Nylon-6 composite in Figure 5.3.

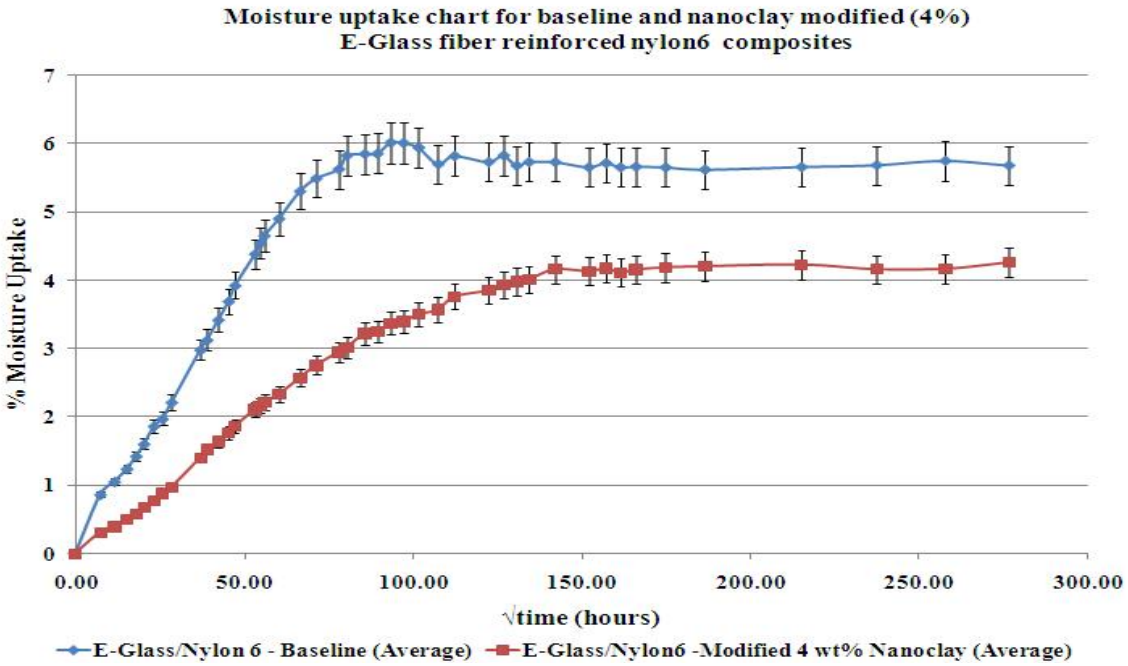

Figure 5.1 Moisture uptake chart for baseline and nanoclay modified (4wt%) E-Glass/Nylon-6 composite

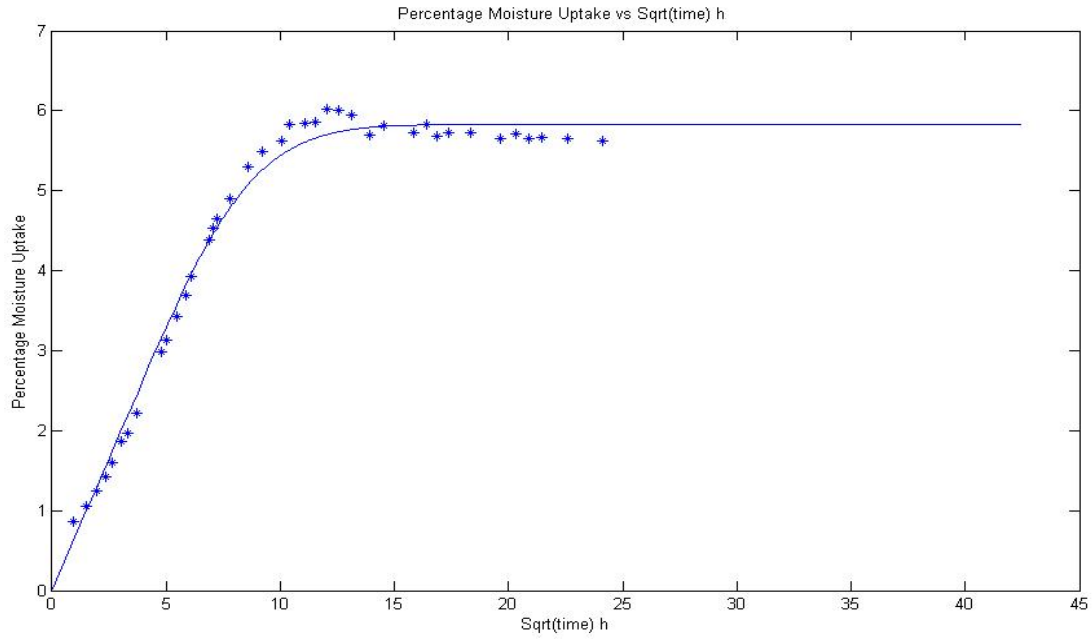

Figure 5.2 Ficks law fit for average moisture uptake in baseline E-Glass/Nylon-6

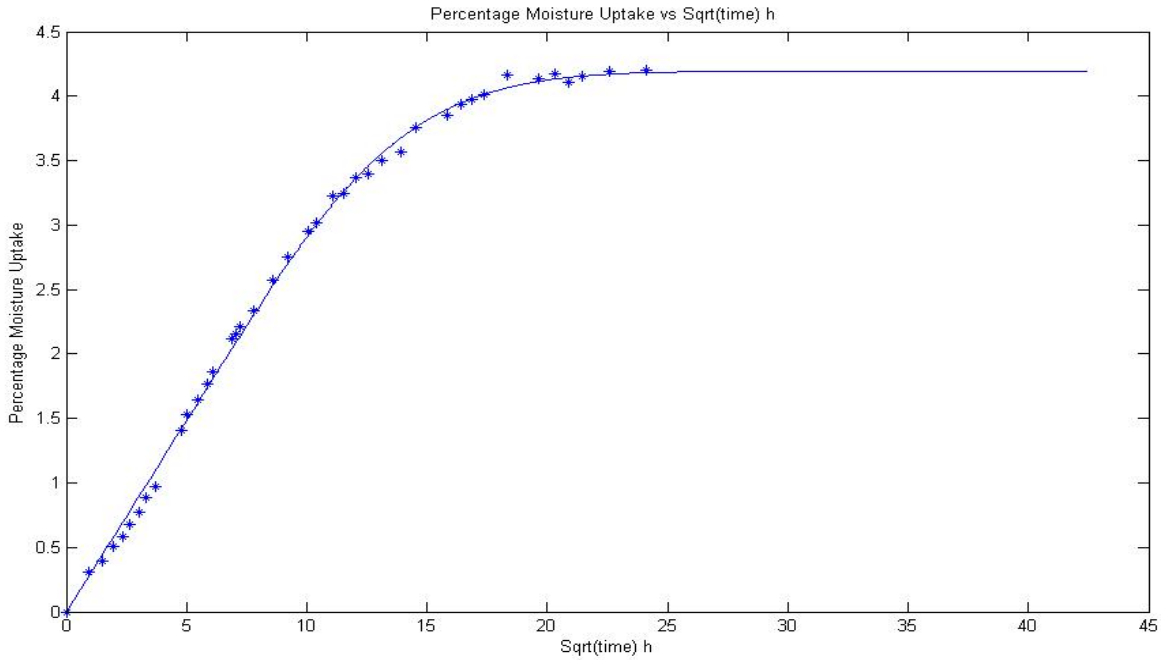

Figure 5.3 Ficks law fit for average moisture uptake for 4 wt%nanoclay modified E-Glass/Nylon-6 composite

Table 5.1 Diffusivity data for baseline and nanoclay modified E-Glass/Nylon-6 composites

Averaged properties after hygrothermal ageing	E-Glass/Nylon-6 (Baseline)	E-Glass/Nylon-6 (4% nanoclay)
Diffusivity (cm^2/sec)	18.138×10^{-8}	7.0064×10^{-8}
M_∞ (grams)	0.7664	0.5492

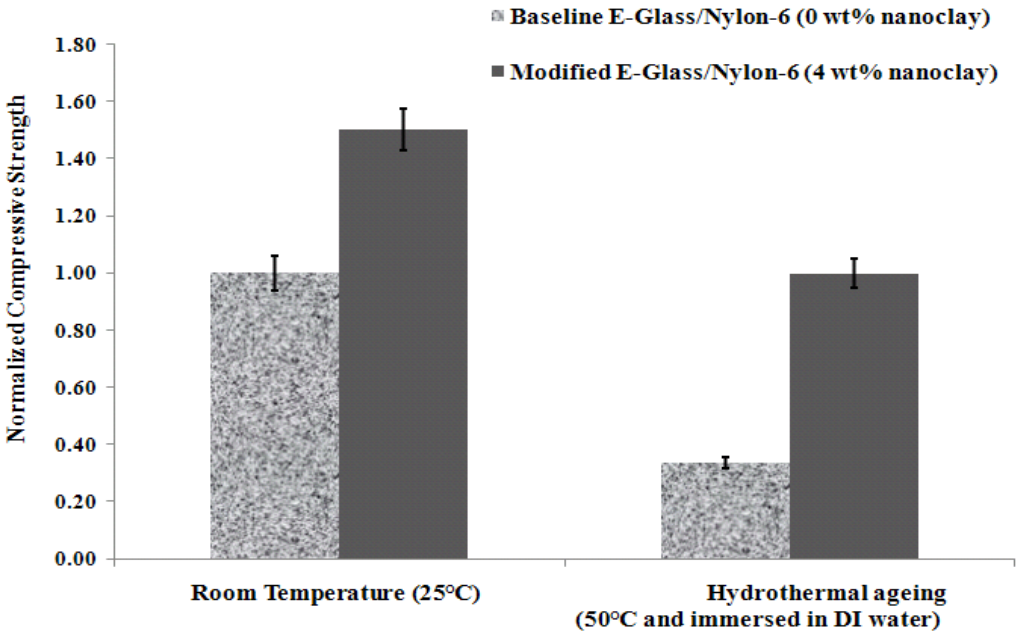

Figure 5.4 Normalized compressive strength for baseline and nanoclay modified (4 wt%) E-Glass/Nylon6 after ~125 hours of hygrothermal ageing

Compression test

Baseline and nanoclay modified (4 wt%) E-Glass/Nylon-6 coupons with were characterized in compression to study the effect hygrothermal ageing on degradation of mechanical properties. The results showed significant improvement in compressive strength with 4 wt% addition of nanoclay compared to baseline E-Glass/Nylon-6 composite after approximately 125 hours of hygrothermal aging, as shown in the bar chart in Figure 5.4.

Short Beam Shear test

Baseline and nanoclay modified (4 wt%) E-Glass/Nylon-6 coupons with were characterized in shear to study the effect hygrothermal ageing on degradation of mechanical properties. The results showed significant improvement (~56%) in interlaminar shear strength with 4 wt%

addition of nanoclay compared to baseline E-Glass/Nylon-6 composite after approximately 125 hours of hygrothermal aging, as shown in the bar chart in Figure 5.5.

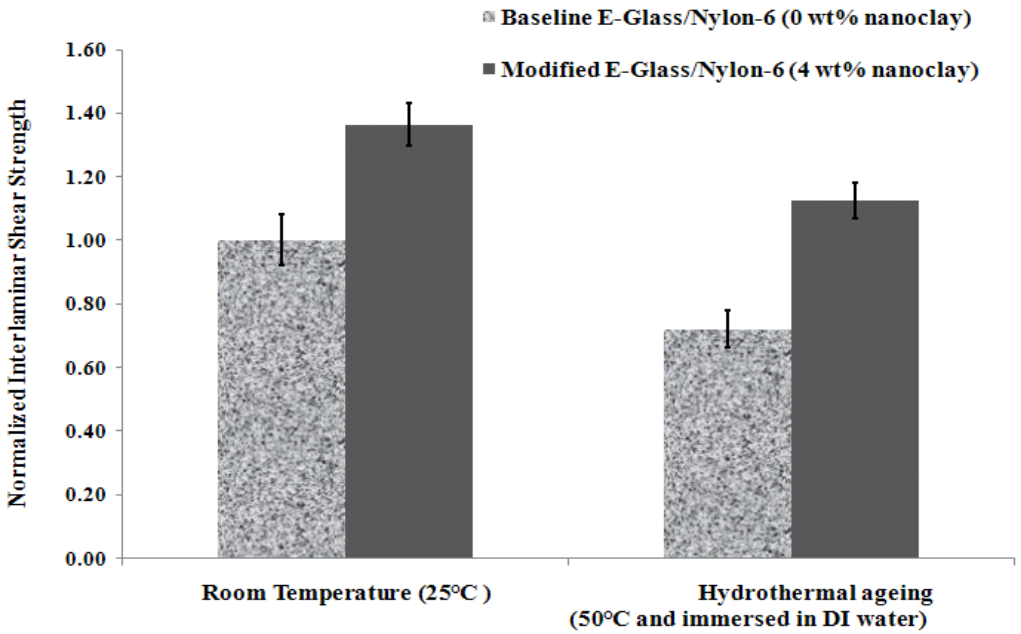

Figure 5.5 Normalized short beam shear strength of baseline and nanoclay modified (4 wt%) E-Glass/Nylon6 after ~125 hours of hygrothermal ageing

The normalized mechanical property data for baseline and nanoclay modified (4 wt%) E-Glass/Nylon-6 nanocomposites after approximately 125 hours of hygrothermal ageing are summarized in Table 5.2.

Table 5.2 Comparison of mechanical properties for E-Glass/Nylon-6 composites after hygrothermal ageing

Averaged Mechanical Properties after hygrothermal ageing	E-Glass/Nylon-6 (0 wt % nanoclay)	E-Glass/Nylon-6 (4 wt % nanoclay)
Normalized Compressive Strength	1	1.97
Normalized Shear Strength	1	1.56

As evident from the experimental results, the addition of silicate layered clay significantly influences the diffusivity of moisture in the nanoclay reinforced Nylon-6 silicate layered nanocomposite. In order understand the underlying mechanism of moisture diffusion in the presence of silicate layered nano-fillers an additional study was performed on neat Nylon-6 resin with different weight addition of silicate layered clay particles, without any E-Glass fiber reinforcement. The study was performed on Nylon-6 baseline and silicate layered clay modified Nylon-6 with 4 wt% and 8 wt% nanoclay loading. The baseline and Nylon-6 silicate layered nanocomposites specimens were 1 in. x 1in. x 0.08 in. in dimensions and hygrothermally aged by completely immersing the specimens in de-ionized water at 50 °C. The moisture diffusion for Nylon-6 resin was observed to follow Fickian diffusion and a curve fit using Ficks law as shown in the moisture uptake chart in Figure 5.6. The diffusivity of 4 wt % nanoclay loading is almost halved, as shown in Table 5.3, with respect to baseline Nylon-6 exhibiting improved barrier resistance. The saturation moisture uptake for nanoclay (4 wt %) modified nylon6 was reduced by ~42% and for nanoclay (8 wt %) modified nylon-6 was reduced by ~45% compared to saturation moisture uptake for baseline Nylon-6. (see Table 5.3)

Table 5.3 Diffusivity data for baseline and nanoclay modified Nylon-6 resin

Averaged properties after hygrothermal ageing	Nylon-6 (Baseline)	Nylon-6 (4 wt% nanoclay)	Nylon-6 (8 wt% nanoclay)
Diffusivity (cm^2/sec)	4.19×10^{-8}	2.13×10^{-8}	1.44×10^{-8}
M_∞ (grams)	0.2502	0.1444	0.1383

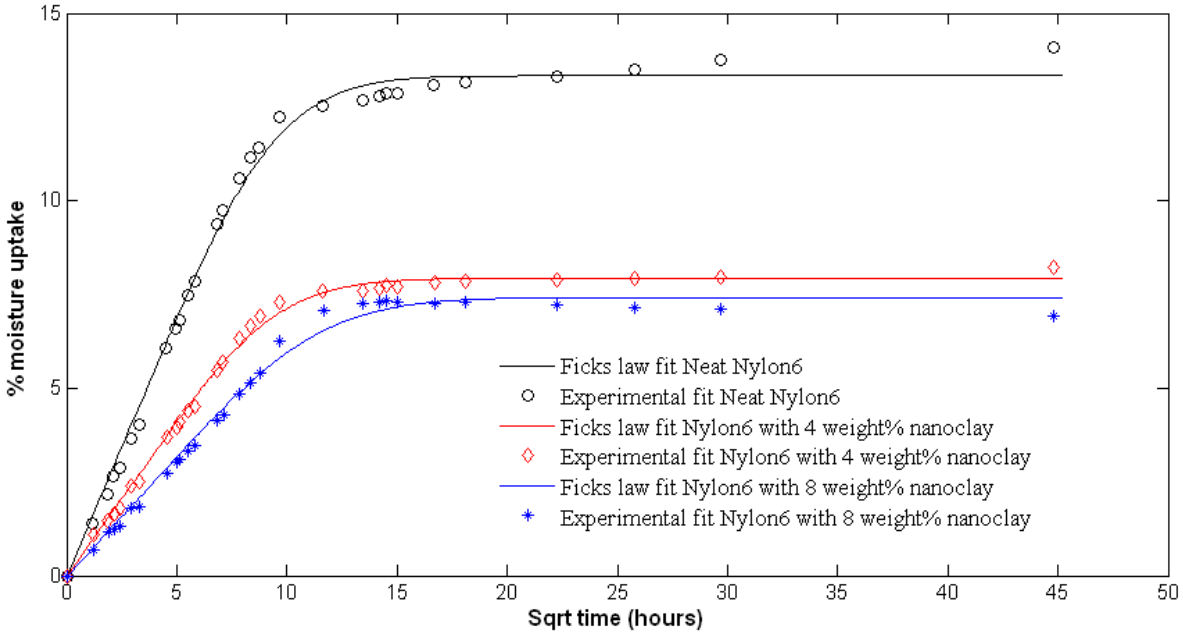

Figure 5.6 Moisture uptake chart for baseline and nanoclay modified Nylon-6 composite

5.2 X-Ray Diffraction Analysis

X-ray diffraction (XRD) is a versatile, non-destructive technique that reveals detailed information about the chemical composition and crystallographic structure of natural and manufactured materials. When a monochromatic X-ray beam with wavelength *lambda* is projected onto a crystalline material at an angle *theta*, diffraction occurs only when the distance traveled by the rays reflected from successive planes differs by a complete number *n* of wavelengths. By varying the angle *theta*, the Bragg's Law conditions are satisfied by different *d*-spacings in polycrystalline materials. Plotting the angular positions and intensities of the resultant diffracted peaks of radiation produces a pattern, which is characteristic of the specimen. Where a mixture of different phases is present, the resultant diffractogram is formed by addition of the individual patterns. Based on the principle of X-ray diffraction, a wealth of structural, physical and chemical information about the material investigated can be obtained.

A standard test for determining the efficiency of the dispersion of nanoclay particles is the non-destructive X-Ray Diffraction (XRD) test. The XRD test measures the degree of dispersion by measuring the scattered pattern formed when a scan of X-Ray beams encounters the nanocomposite. XRD measurements were carried out using Philips XRG 3100 equipped with CuKα radiation operating at 40kV and 35mA. The diffraction patterns were collected between angles (2θ) of 0.5-10° at a scanning rate and step size of 0.010/sec and 0.02°, respectively. These measurements are used to estimate the distance between individual platelets (d_{001}) after compounding. The XRD pattern will result in fewer reflections of corresponding silicate layered clay peak with complete exfoliation and uniform dispersion of nanoclay in the composite.

XRD was performed on both E-Glass/Nylon-6 with 4 wt% and 8 wt% silicate layered clays to characterize the nanostructure morphology. Also, XRD patterns (Figure 5.7) were obtained for E-Glass/Nylon-6 without silicate layered clay, for reference. The characteristic [001] diffraction peak of organically modified MMT (I.24TL) appeared at 2θ = 5.05°. Therefore, the basal spacing of I.24TL platelets was determined to be 1.75 nm, according to Bragg's Law. We can observe that the characteristic [001] peak of I.24TL is absent in modified nylon-6 nanocomposites around 2θ = 5.05°. The absence of these characteristic [001] peaks for I.24TL nanoclay in XRD pattern of E-Glass/Nylon-6 with 4 wt% addition of nanoclay at low 2 theta angles indicates exfoliated nanoclay morphology. However, the XRD pattern for E-Glass/Nylon-6 with 8 wt% addition nanoclay shows the characteristic [001] peak for I.24TL nanoclay shifted to low 2 theta angles at a 2θ value of 0.68. The shift in characteristic [001] peak for I.24TL nanoclay to low 2 theta angles indicates that the basal spacing of MMT platelets has increased from 1.75 nm to approximately 13 nm, potentially indicating partially exfoliated nanoclay morphology compared with 4% nanoclay loading. It is postulated that the complete uniform dispersion of 8 wt% MMT

nanoclay was hindered due to the increased viscosity of the Nylon-6 resin system at higher nanoclay loading.

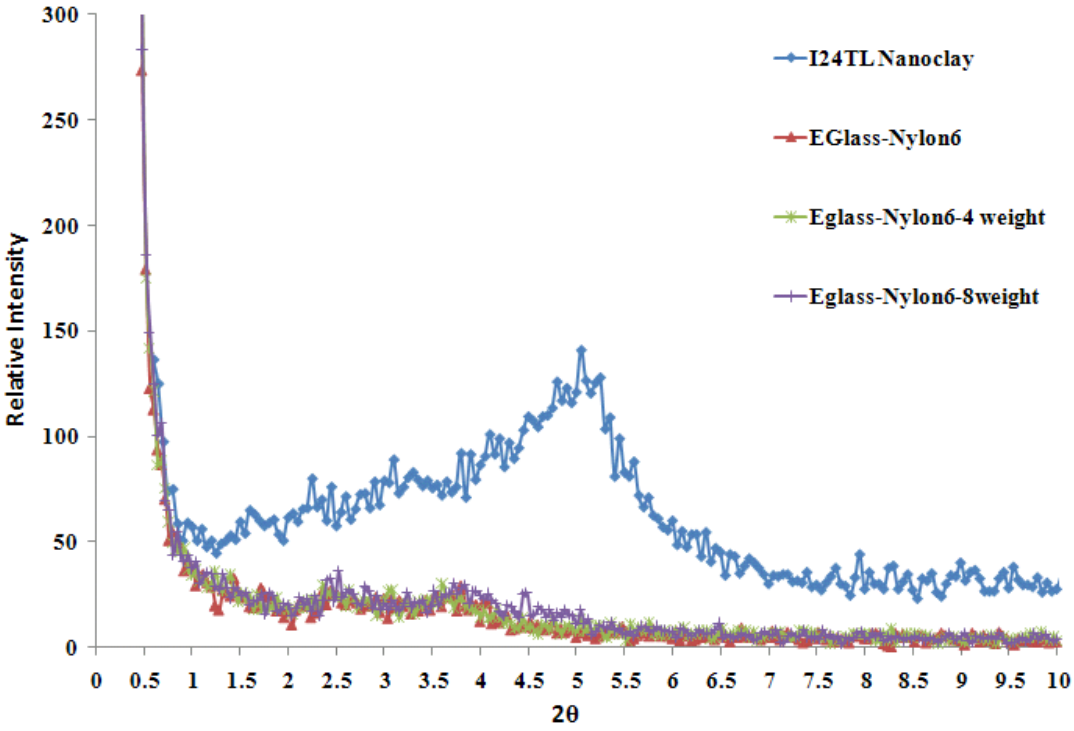

Figure 5.7 XRD pattern for E-Glass/Nylon-6 nanocomposites

5.3 Analytical Model

An analytical model is developed to describe the mechanism of moisture diffusion in silicate layer thermoplastic nanocomposites is attempted. It is important to realize that the diffusivity through a heterogeneous media contains impenetrable silicate layered clay, which is assumed to be well dispersed though randomly oriented. This morphology strongly influences the diffusion process because of its orientation, concentration and with interactions with the host polymer. The presence of silicate layered clay creates a tortuous path for the permeant molecules to diffuse into the bulk of the polymer, creating an increased path for the permeant, and also reduces the

volume of material available for flow because they are impenetrable. Nielsen (1967) had proposed a two dimensional model for gas and liquid diffusion in a polymer with impenetrable filler. The proposed equation focuses on the tortuous path created and the aspect ratio of the impenetrable filler. This model prediction agrees well for crystalline polymer films. Subsequently, Liu *et al* (2007) proposed a three dimensional diffusion model for bulk amorphous polymer capturing the effect of tortuosity and aspect ratio of randomly oriented and exfoliated layered silicate clays. Further, the addition of organically modified layered silicate clays binds the clay to the polymer, thereby creating constrained polymer regions. Basically, constrained region induces restricted motion of the polymer. Consequently, the effect is that the constrained region is that it reduces the free volume, within a polymer especially in amorphous polymers. Free volume can be defined as the fraction of volume not occupied by the polymer. The proposed formulation is an attempt to capture the influence of both the tortuosity effect and reduction in free volume due to addition of organically modified layered silicate clay to a polymer.

Doolittle's empirical equation relates the polymer viscosity to free volume, which is applied to polymers in their rubbery range. Roy *et al*. (1989) extended the Doolittle equation to propose its diffusion counterpart

$$D = \frac{D_o}{T_o} T e^{\{-B^D\left(\frac{1}{f}-\frac{1}{f_o}\right)\}} \quad \text{- (3)}$$

Where

D- Diffusion co-efficient

D_o- Diffusion co-efficient at reference temperature

T – Ambient Temperature

To- Reference Temperature

B^D- Numerical parameter inversely related to minimum hole size

f- Fractional free volume at given temperature

f_o - Fractional free volume at reference temperature

Assuming the change in fractional free volume is additive (Knauss and Emri)

$$f = f_o + \alpha\, \Delta T + \varepsilon_{kk}^{f} + \gamma C \qquad \text{- (4)}$$

α – Co-efficient of volumetric thermal expansion

ΔT – Change in temperature

ε^f_{kk} – Volume Dilatation of free volume due to external loads

γ – Co-efficient of volumetric swelling

C- Solvent concentration

Eqn (4) is valid in the rubbery range ($T > T_g$), but requires a history dependent convolution integral form in the glassy range,

$$f = f_o + (\alpha * dT) + \varepsilon_{kk}^{f} + (\gamma * C) \qquad \text{- (5)}$$

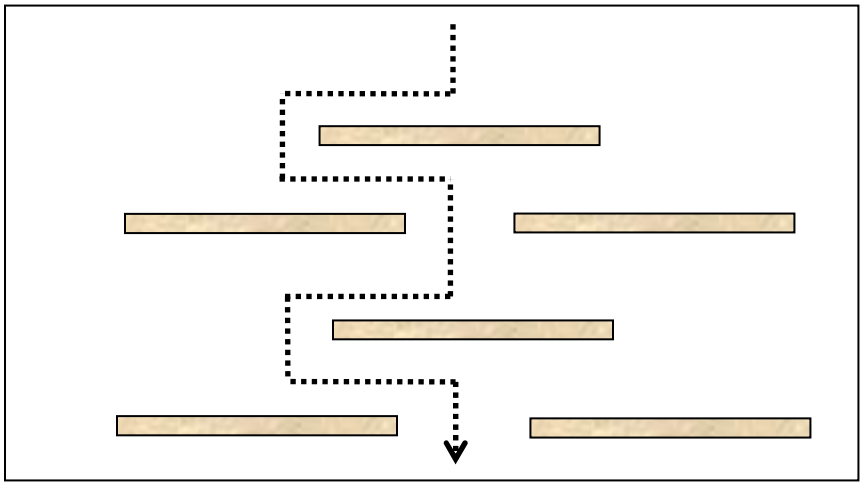

Figure 5.8 Tortuous path for a penetrant molecule in presence of silicate layered clay

Assuming that the addition of nanoclay in an amorphous polymer causes the diffusing molecules to take a tortuous path during diffusion (Figure 5.8), as the clay platelets are impermeable, we can introduce a tortuosity factor (τ), which is defined as

$$\tau = \left(\frac{d}{d'}\right)^2$$

Where d' is the effective distance that the diffusing molecules must travel, and d is the shortest distance the molecules would travel in the absence of the clay platelets. Hence the Doolittle equation is modified to accommodate the tortuosity factor (τ) and can be rewritten as

$$D = \tau \frac{D_o}{T_o} T e^{\{-B^D\left(\frac{1}{f}-\frac{1}{f_o}\right)\}} \quad \text{- (6)}$$

Also, let us assume that the addition of nanoclay in an amorphous polymer results in a constrained region surrounding the nanoclay platelets. In such an event Eqn (3) needs to rewritten as

$$f_c = Kf \qquad \text{where, } 0<K<1 \quad \text{- (7)}$$

Where f_c is constraint free volume and the nanoscale free volume constraint factor K is given by

$$K = 1 - K_o \varphi^n \quad \text{- (8)}$$

Where

K_o – Free Volume Constraint Co-efficient

φ – Nanoclay loading in volume percent, i.e. ratio of weight percent nanoclay loading and density of material

n- Exponent of φ

Substituting Eqns (5), (7) and (8) in Eqn (6) we have

$$D_c = \tau \frac{D_o}{T_o} T e^{\{-B^D\left(\frac{1}{f_c}-\frac{1}{f_{oc}}\right)\}} \quad \text{- (9)}$$

But,

$$\frac{1}{f_c} - \frac{1}{f_{oc}} = \frac{-K[\left(\alpha * dT\right)+\varepsilon_{kk}^f+(\gamma * C\Big)]}{K^2 f f_o} = \frac{-\left(\alpha * dT\right)+\varepsilon_{kk}^f+(\gamma * C\Big)}{K f_o (f_o+(\alpha * dT)+\varepsilon_{kk}^f+(\gamma * C))} \quad \text{- (10)}$$

Substituting Eqn (10) in Eqn (9)

$$D_c = \tau \frac{D_o}{T_o} T e^{\left\{\frac{B^D \quad \left(\alpha * dT\right)+\varepsilon_{kk}^f+(\gamma * C\Big)}{K f_o (f_o+(\alpha * dT)+\varepsilon_{kk}^f+(\gamma * C))}\right\}} \quad \text{- (11)}$$

In order to use B^D, f_o, and α from WLF equation it is convenient to set T_o=T_g

In order to evaluate the free volume constraint parameter K, the diffusivity of a polymer specimen needs to be measured at two different nanoclay loadings, as well as zero nanoclay loading

Define,

D_u - Diffusion co-efficient of unconstrained zone (zero nanoclay loading)

D_1 - Diffusion co-efficient of constrained zone (corresponding to nanoclay loading of φ_1)

T_1- Reference Temperature

Then from Eqn (8), assuming no applied mechanical load ($\varepsilon_{kk}^f = 0$),

$$\ln D_u - lnD_1 = \ln\left(\frac{D_o T_1}{T_g}\right) - \ln\left(\frac{D_o T_1}{T_{g1}}\right) - ln\ \tau_1 + \{\left(1-\frac{1}{K}\right)\frac{B^D}{f_o}\frac{[(\alpha * dT)+(\gamma * C)\ ]}{(f_o+(\alpha * dT)+(\gamma * C)}\}$$

where $\tau_1 = \frac{1}{(1+\left(\frac{2\varsigma\varphi_1}{3\pi}\right))^2}$

and ς is aspect ratio of nanoclay platelets (Liu *et al*, 2007)

or, $\tau_1 = 1 + \left(\frac{L}{2W}\right)\varphi_F$

where L is the length of face of filler platelets, W is the thickness of the filler platelets and φ_F is the volume fraction of filler (Nielsen, 1967)

$$\ln D_u - lnD_1 = \ln\left(\frac{D_o T_1}{T_g}\right) - \ln\left(\frac{D_o T_1}{T_{g1}}\right) - ln\,\tau_1 + \{\left(1 - \frac{1}{1-K_0\varphi_1^n}\right)\frac{B^D}{f_o}\frac{[(\alpha*dT)+(\gamma*C)\,]}{(f_o+(\alpha*dT)+(\gamma*C)}\}$$

giving,

$$\ln D_u - lnD_1 - \ln\left(\frac{D_o T_1}{T_g}\right) + \ln\left(\frac{D_o T_1}{T_{g1}}\right) + ln\,\tau_1 = \left(\frac{-K_0\varphi_1^n}{1-K_0\varphi_1^n}\right)\frac{B^D}{f_o}\frac{[(\alpha*dT)+(\gamma*C)\,]}{(f_o+(\alpha*dT)+(\gamma*C)} \quad \text{- (12)}$$

Solving equation (10) for $K_o\varphi^n$,

$$\ln D_u - lnD_1 - \ln\left(\frac{D_o T_1}{T_g}\right) + \ln\left(\frac{D_o T_1}{T_{g1}}\right) + ln\,\tau_1 = K_0\varphi_1^n\left(\ln D_u - lnD_1 - \ln\left(\frac{D_o T_1}{T_g}\right) + \ln\left(\frac{D_o T_1}{T_{g1}}\right)\right) - K_0\varphi_1^n\{\frac{B^D}{f_o}\frac{[(\alpha*dT)+(\gamma*C)\,]}{(f_o+(\alpha*dT)+(\gamma*C)}\}$$

$$K_0\varphi_1^n = \frac{\ln D_u - lnD_1 - \ln\left(\frac{D_o T_1}{T_g}\right) + \ln\left(\frac{D_o T_1}{T_{g1}}\right) + ln\,\tau_1}{\left(\ln D_u - lnD_1 - \ln\left(\frac{D_o T_1}{T_g}\right) + \ln\left(\frac{D_o T_1}{T_{g1}}\right) + ln\,\tau_1\right) - \{\frac{B^D}{f_o}\frac{[(\alpha*dT)+(\gamma*C)\,]}{(f_o+(\alpha*dT)+(\gamma*C)}\}}$$

The right hand side is completely known and is a constant

$$\beta_1 = \frac{\ln D_u - lnD_1 - \ln\left(\frac{D_o T_1}{T_g}\right) + \ln\left(\frac{D_o T_1}{T_{g1}}\right) + ln\,\tau_1}{\left(\ln D_u - lnD_1 - \ln\left(\frac{D_o T_1}{T_g}\right) + \ln\left(\frac{D_o T_1}{T_{g1}}\right) + ln\,\tau_1\right) - \{\frac{B^D}{f_o}\frac{[(\alpha*dT)+(\gamma*C)\,]}{(f_o+(\alpha*dT)+(\gamma*C)}\}}$$

Therefore Eqn (10) becomes

$$K_0 \varphi_1^n = \beta_1 \quad \text{- (13)}$$

Now taking $\log_{10}$ on both sides we have

$$log_{10} K_0 + n\, log_{10}\, \varphi_1 = log\, \beta_1 \quad \text{- (14)}$$

Repeating the diffusivity measurement using another nanoclay loading, φ_2, and a corresponding tortuosity τ_2, would result in a similar equation

$$log_{10} K_0 + n\, log_{10}\, \varphi_2 = log\, \beta_2 \quad \text{- (15)}$$

Again, the right hand side is completely known and is a constant given by,

$$\beta_2 = \frac{\ln D_u - lnD_2 - \ln\left(\frac{D_o T_2}{T_g}\right) + \ln\left(\frac{D_o T_2}{T_{g2}}\right) + ln\, \tau_2}{\left(\ln D_u - lnD_2 - \ln\left(\frac{D_o T_2}{T_g}\right) + \ln\left(\frac{D_o T_2}{T_{g2}}\right) + ln\, \tau_2\right) - \left\{\frac{B^D \ [(\alpha * dT) + (\gamma * C)\ ]}{f_o\,(f_o + (\alpha * dT) + (\gamma * C)}\right\}}$$

where $\tau_2 = \frac{1}{(1+\left(\frac{2\varsigma\varphi_1}{3\pi}\right))^2}$

and ς is aspect ratio of nanoclay platelets (Liu *et al*, 2007)

or $\tau_2 = 1 + \left(\frac{L}{2W}\right)\varphi_F$

Where L is the length of face of filler platelets, W is the thickness of the filler platelets and φ_F is the volume fraction of filler (Nielsen, 1967)

Eqns (14) and (15) can now be solved for constants K_o and n. Of course, additional nanoclay loadings will result in a better least squares fit for K_o and n. Based on our test data, the values of K_o and n are show in Figure 5.9.

After solving for the constants the constraint factor (K) is plotted, Figure 5.9, against the weight addition nanoclay loading for layered silicate clay with different aspect ratio for two different tortuosity models.

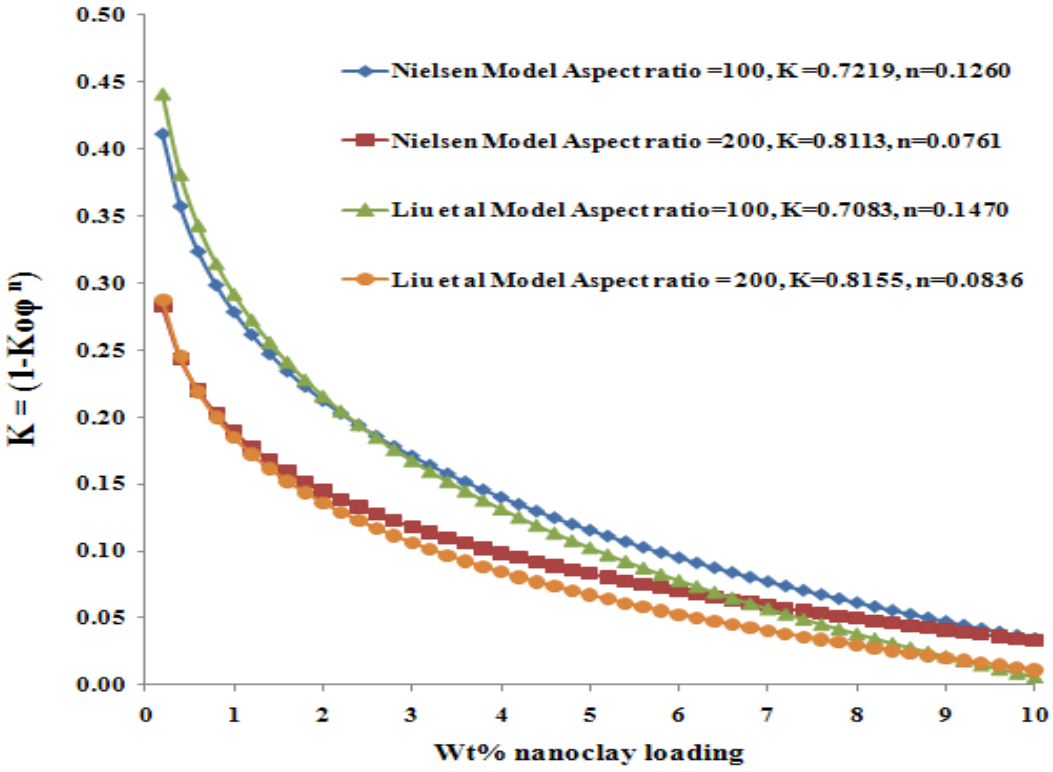

Figure 5.9 Constrained factor (K) versus clay content

It can be seen that the constraint factor (K) is significantly influenced by the aspect ratio of layered silicate clays. The two models lie on top of each other at low layered silicate clay loadings (< 4 wt%); however at higher clay loadings, Nielsen's model tends to plateau at a higher constrained factor value compared with Liu's model.

Adam and Beall (2009) had suggested that the free volume of constrained and unconstrained polymer regions are significantly different and hence can be indirectly confirmed by AFM. Ultra thin sections of Nylon-6 neat resin and with nanoclay modified Nylon-6 nanocomposites cross-

sections were cut using an ultra microtome equipped with a diamond knife and the sections were supported on carbon film on copper grids. Film thickness was of Nylon-6 neat resin was 400 nm and the film thickness of nanoclay modified nanocomposites were 200 nm. The three dimensional AFM images for Nylon-6 with 0 wt%, 4 wt% and 8wt% silicate layered clay loading are shown in Figure 5.10 (a), Figure 5.11 (a) and Figure 5.12 (a) respectively. Also, the two dimensional AFM images for Nylon-6 with 0 wt%, 4 wt% and 8wt% silicate layered clay loading are shown in Figure 5.10 (b), Figure 5.11 (b) and Figure 5.12 (b) respectively.

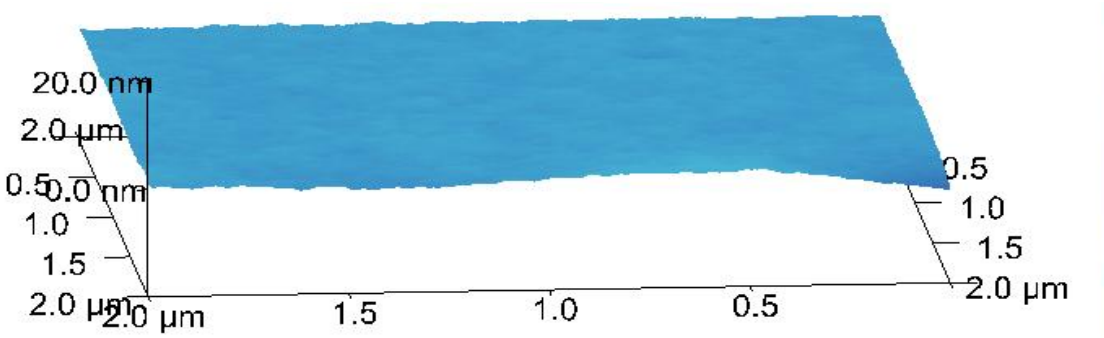

Figure 5.10 (a) Three dimensional AFM image of Nylon-6 with 0 wt % nanoclay

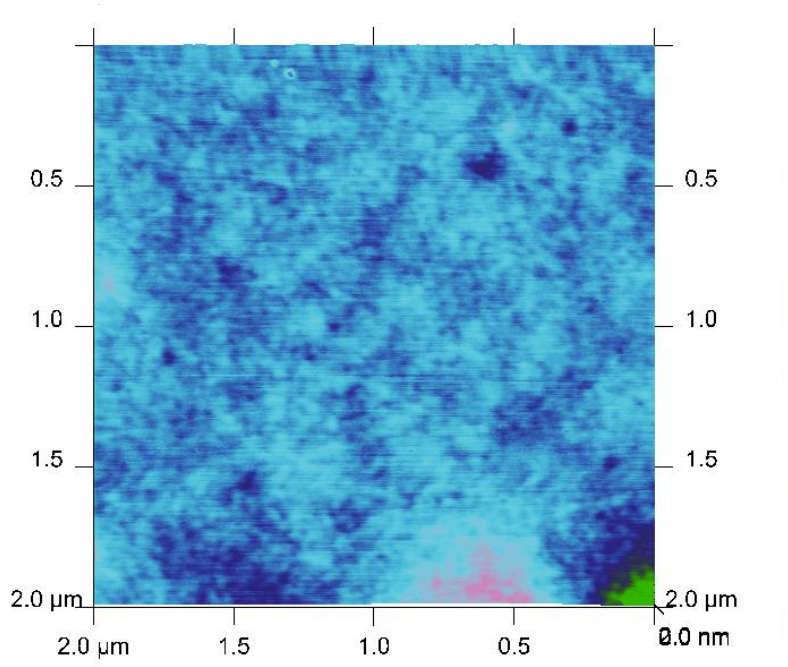

Figure 5.10 (b) Two dimensional AFM image of Nylon-6 with 0 wt % nanoclay

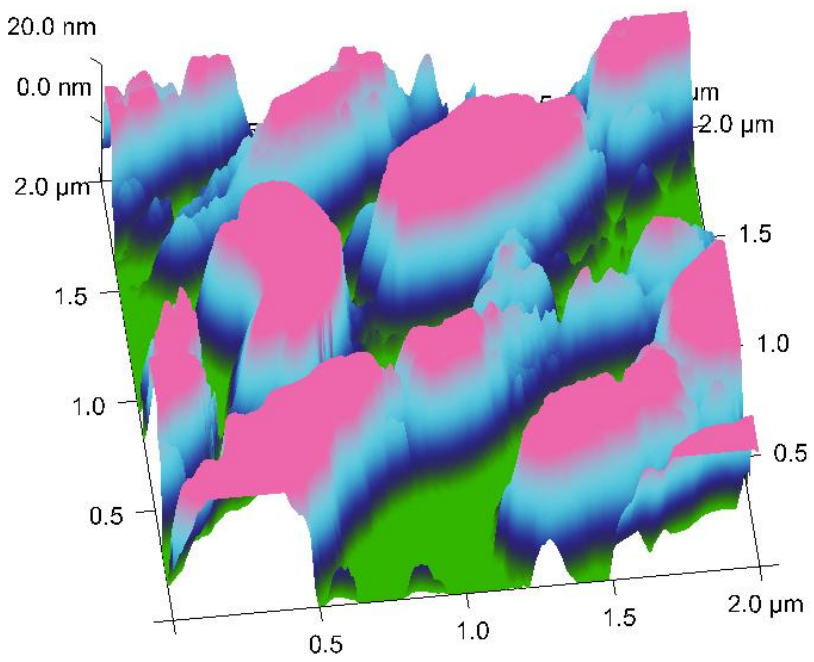

Figure 5.11 (a) Three dimensional AFM image of Nylon-6 with 4 wt % nanoclay

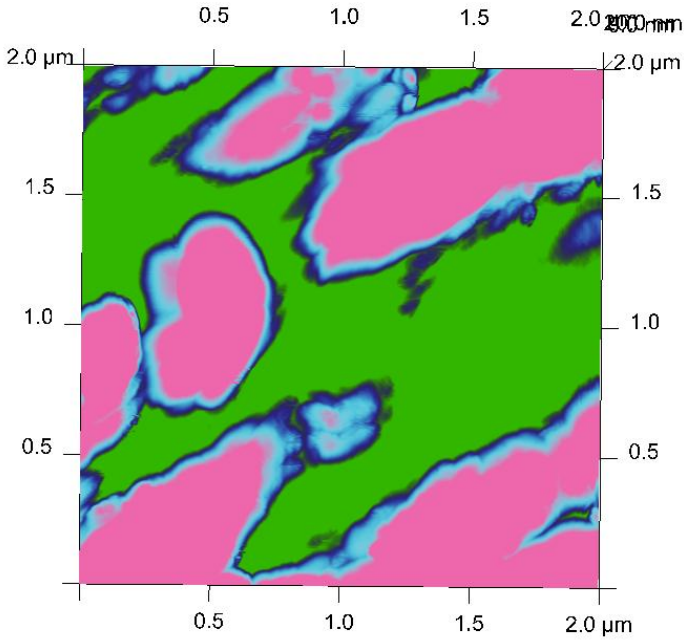

Figure 5.11 (b) Two dimensional AFM image of Nylon-6 with 4 wt % nanoclay

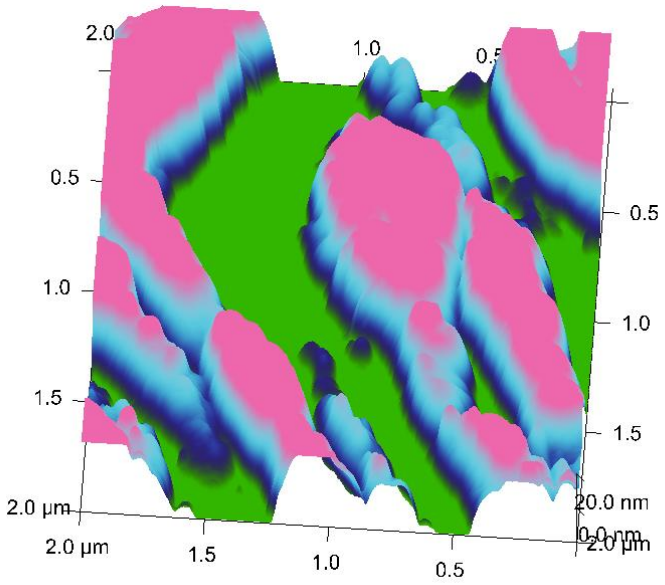

Figure 5.12 (a) Three dimensional AFM image of Nylon-6 with 8 wt % nanoclay

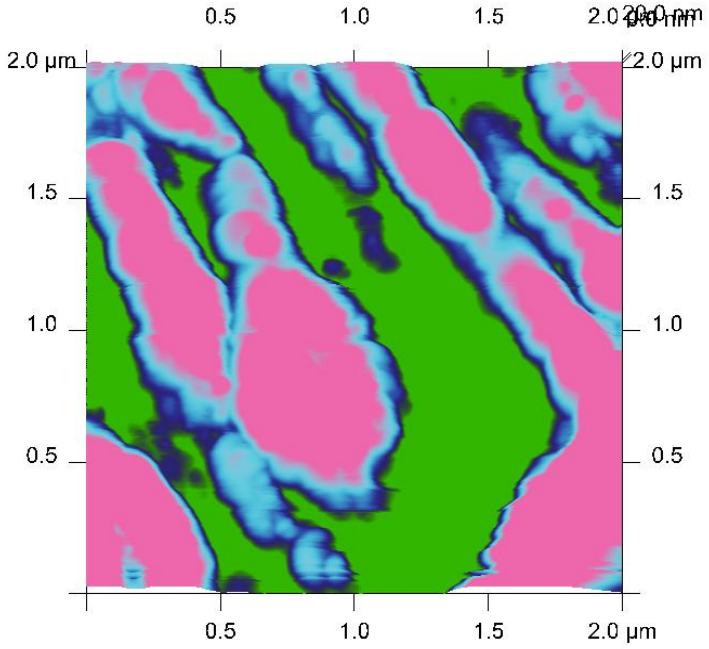

Figure 5.12 (b) Two dimensional AFM image of Nylon-6 with 8 wt % nanoclay

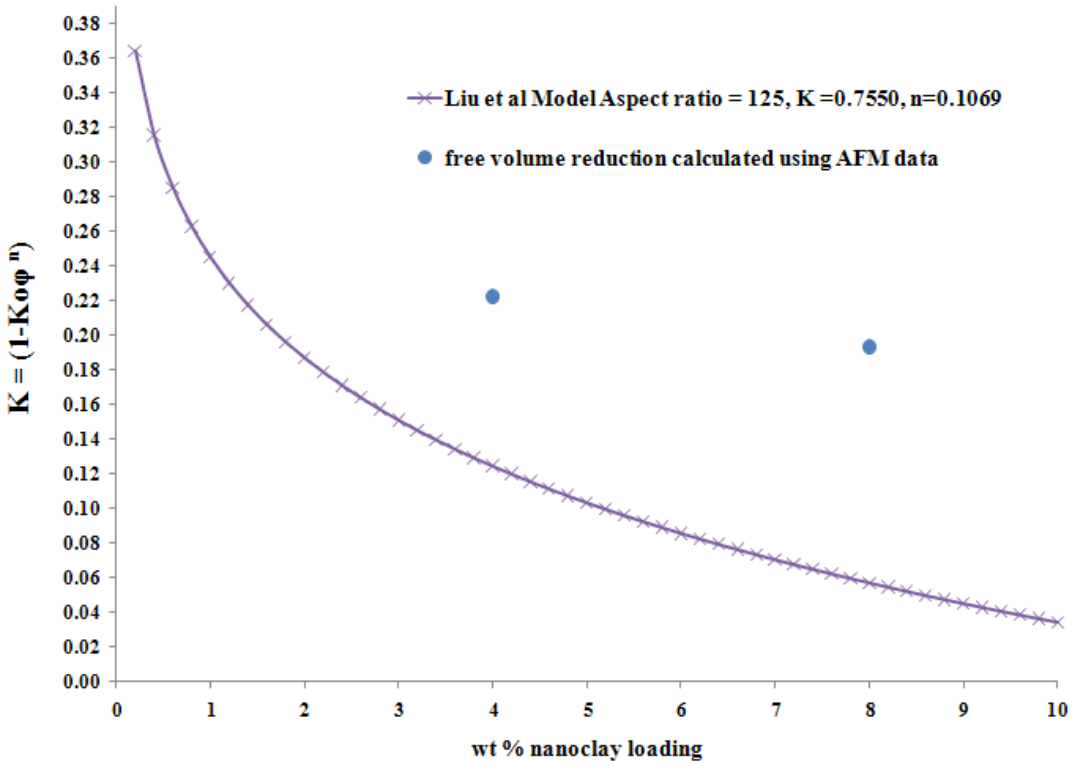

Figure 5.13 Comparison of free volume reduction computed using analytical model and experimental data using AFM

It can be observed from the AFM images that Nylon-6 with 0 wt% nanoclay (Figure 5.10 (a) & (b)) has relatively a smooth surface morphology compared to Nylon-6 with silicate layered clay loading of 4 wt% and 8 wt%, shown in Figures 5.11 (a) & (b), and 5.12 (a) & (b) respectively. The unconstrained regions tend to appear as high plateaus and it can be observed that more hills and valleys are prominent in both 4 wt% silicate layered clay loading and 8 wt% loading, where valleys correspond to constrained regions. The presence of a larger constrained region zone at a higher clay loading corroborates quantitatively the proposed power law behavior of constraint factor K with the volume fraction of layered silicate clay fillers.

The addition of nanofillers to a neat resin creates constraint regions in the polymer, thereby resulting in a reduction of free volume in the nanofiller modified polymer. The reference cubic

volume of material was calculated. Subsequently, the missing volume of the material is calculated using the AFM data for baseline Nylon-6 and nanoclay modified Nylon-6 with 4 wt% and 8 wt% nanoclay loading. The resulting volume fraction of loss in free volume is computed. The volume fraction of loss in change in free volume calculated from AFM experiments is compared with results from the analytical model as shown in Figure 5.13. The results indicate that the loss in change in free volume is comparable to (within ~15% error) results using the analytical model.

CHAPTER 6

CONCLUSIONS

As mentioned previously, the overall compressive strength of a polymer matrix composite is only about 50% of its tensile strength. The strength of the surrounding polymer matrix plays a key role in characterizing the critical buckling load of the fibers by constraining the fibers from buckling. In this work, unidirectional E-Glass fiber reinforced PP with surfactant modified montmorillonite nanoclay as nano-reinforcement were fabricated using pultrusion and E-Glass fiber reinforced Nylon-6 composite and nanocomposites were prepared using thermoplastic compression molding in which the matrix was Nylon-6 with surfactant modified montmorillonite nanoclay as nano-reinforcement. Based on the research and experimental data, the compressive properties of E-Glass/PP showed a monotonic increase in compressive strength (110%), short beam shear strength (60%) and a minor improvement of 3.4% in tensile strength with 3 wt% nanoclay loading. E-Glass/Nylon-6 exhibited a significant improvement in compressive strength (50%), short beam shear strength (~36%) and a marginal increase of 3% in tensile strength with 4 wt% nanoclay loading. Unlike the trend in E-Glass/PP nanocomposites the compressive strength and inter-laminar shear strength in E-Glass/Nylon-6 nanocomposites showed a peak improvement in compressive strength (50%) and short beam shear strength (~36%) with 4 wt% nanoclay loading. At 8 wt% nanoclay loading, the increase in compressive strength was 34%, and for short beam shear strength the increase was only 3%.

Hygrothermal analysis confirmed that the diffusivity and saturation moisture uptake for nanoclay (4 wt%) modified E-Glass/Nylon-6 was significantly reduced (61% and 30% respectively) as compared with moisture uptake in baseline E-Glass/ Nylon-6 composites. Moisture diffusion

followed Fickian behavior in both baseline E-Glass/Nylon-6 and nanoclay (4 wt%) modified E-Glass/Nylon-6 nanocomposites. Further, mechanical tests after hygrothermal ageing indicate that the degradation of mechanical properties in nanoclay (4 wt%) modified E-Glass/Nylon-6 was significantly less compared with baseline (0 wt%) E-Glass/Nylon-6 composites exposed to the same environmental conditions. In fact, it is interesting to note that the compressive and inter-laminar shear strength of E-Glass/Nylon-6 with 4 wt% addition of nanoclay after approximately 125 hours of hygrothermal ageing are comparable with the compressive and inter-laminar shear strength of dry (unaged) baseline E-Glass/Nylon-6 composite with 0 wt% clay. In other words, the addition of 4 wt % nanoclay helps significantly in redressing the deleterious effect of hygrothermal degradation in E-Glass/Nylon-6 composite through its effectiveness as a diffusion barrier.

An analytical model is developed to describe the mechanism of moisture diffusion in silicate layer thermoplastic nanocomposites. The addition of nano-fillers to a neat resin creates tortuous path and constraint regions in the polymer, thereby resulting in a reduction of free volume in the nano-filler modified polymer. The model captures the diffusion mechanism and attributes the change in diffusivity and moisture uptake with weight addition of layered silicates to tortuosity and reduction in free volume created by the presence of nanoclay platelets. Also, the loss in change in free volume was computed based on AFM images and compared with the analytical model.

The present study also underscores the fact that the improvement in properties through the addition of surfactant modified nanoclay potentially manifests itself over a wide range of thermoplastic resin systems (PP, Nylon-6) providing significant improvement in mechanical

(compressive and inter-laminar shear) as well as diffusion barrier properties. Further, mechanical characterization experiments on carbon fiber reinforced aerospace grade thermoplastic resins, such as, PEEK and PPS, with fiber volume fractions greater than 50% would provide insight on the effect of addition of nanoclay in aerospace grade thermoplastic resins . Also, multi-scale simulations of nanoclay/polymer interface behavior are currently in progress in order to understand the underlying strength enhancement mechanisms. Through these investigations, the authors seek to establish that the addition of surfactant modified nanoclay could yield significant improvement in mechanical and diffusion barrier properties over a wide range of thermoplastic resin systems and fiber reinforcement type, and for different fiber volume fractions.

REFERENCES

Adame, D., Beall, G. W., (2009). Direct measurement of the constrained polymer region in polyamide/clay nanocomposites and the implications for gas diffusion, *Applied Clay Science*, Vol. 42, pp. 545–552.

Argon, A.S. (1972). Fracture of Composites. Treatise on Material Science and Technology, Vol. 1, Academic Press, New York, pp. 79-114.

Budiansky, B. (1983). Micromechanics. Computers and Structures, Vol.16, pp. 3-12.

Budiansky, B., and Fleck, N.A. (1993).Compressive Failure of Fiber Composites. *Journal of Mechanics and Physics of Solids*, Vol. 41, 183-211.

Burnside, S.D., Giannelis, E.P., (2000). Nanostructure and properties of polysiloxane layered silicate nanocomposites. *Journal of Polymer Science*, Vol. B 38, 1595–1601.

Carsson, A. and Astrom B.T. (1998). Expermimental investigation of pultrusion of glass fiber reinforced polypropylene composites. *Composites: Part A*, Vol. 29A, pp.585-593.

Chen, C. and Curliss, D. (2001). Resin Matrix Composites: Organoclay-Aerospace Epoxy Nanocomposites, Part II, *SAMPE Journal*, Vol. 37(5): pp.11-15.

Christopher O.O. and Lerner, M. (2001). Nanocomposites and Intercalation compound. In the Encyclopedia of Physical Science and Technology, 3rd edition, Vol. 10.

Creighton, C.J. and Clyne, T.W. (2000). The compressive strength of highly-aligned carbon-fiber/epoxy composites produced by pultrusion. *Composites Science and Technology*, Vol. 60, pp.525-533.

Creighton, C.J., Sutcliffe, M.P.F. and Clyne, T.W. (2001). A multiple field image analysis procedure for characterization of fiber alignment in composites. *Composites: Part A*, Vol. 32, pp.221-229.

Hussain, F. Derrick, D., and Haque, A. (2005). S2 Glass/Vinyl ester Polymer Nanocomposites: Manufacturing, Structures, Thermal and Mechanical Properties. *Journal of Advanced Materials*, Vol. 37(1), pp 16-27.

Jang, B. Z. (1994). Advanced Polymer Composites: Principle's and Applications. ASM International.

Kozima, Y., Usuki. A., Kawasumi. M., Okada. A., Fukushima. Y., Kurauchi, T., and Kamigaito O.J.(1993). Mechanical Properties of Nylon-6 clay hybrid, *Journal of Material Research,* Vol. 8, pp.1185-1189.

Kojima Y, Fukumori K, Usuki A, Okada A, Kurauchi T. (1993). Journal of Material Science Letter, Vol. 12: 889–890.

Kojima Y, Usuki A, Kawasumi M, Okada A, Kurauchi T, Kamigaito O. (1993). *Journal of Applied Polymer Science*, Vol. 49: 1259–1264.

Kojima Y, Usuki A, Kawasumi M, Okada A, Kurauchi T, Kamigaito O. (1993). *Journal of Polymer Science, Part A: Polymer Chemistry*,Vol. 3: 983–986.

Liskey, A. K. (1989). Pultrusion on a fast track. *Advanced Materials & Processes*, Vol. 135(2): pp.31-35.

Liang, Z.-M., Yin, J., (2003). Poly(etherimide)/montmorillonite nanocomposites prepared by melt intercalation. *Journal of Applied Polymer Science*, Vol. 90, pp.1857–1863.

Liang, Zhu-Mei, Yin, J., Wu, J.-H., Qiu, Z.-X., He, F.-F., (2004). Polyimide/ montmorillonite nanocomposites with photolithographic properties. *European Polymer Journal*, Vol. 40, pp.307–314.

Liu, W., Hoa, S.V., Pugh, M., (2007). Water uptake in epoxy-clay nanocomposites: Model development, *Composites science and technology*, Vol. 67, pp. 3308-3315.

Nielsen, L.E., (1967). Models for the Permeability of Filled Polymer Systems, *Journal of Macromolecular Science (Chemistry)*, Vol. A1(5), pp. 929-942.

Okada. A. and Usuki A. (1995). The Chemistry of Polymer-Clay Hybrids, *Material Science Engineering*, C3, pp.109-115.

Paul, D. R. (2001). Effect of Melt Processing Conditions on the Extent of Exfoliation in Organoclay-Based Nanocomposites. *Polymer*, Vol. 42, 9513-9522.

Promanik, M., Acharya, H., Srivastava, S.K., (2004). Exertion of inhibiting effect by aluminosilicate layers on swelling of solution blended EVA/clay nanocomposite. *Macromolecules Material Engineering*, Vol. 289, pp.562–567.

Rosen, B.W. (1964). Mechanisms of Composite Strengthening. *Fiber Composite Materials*, American Society of Metals, Cleveland. OH, (Chapter 3) 37-75.

Roy , S., Lefebvre, D. R., Dillard, D. A., Reddy, J. N., (1989). A Model for the Diffusion of Moisture in Adhesive Joints. Part III: Numerical Simulations, *The Journal of Adhesion*, Vol. 27, Issue 1 1981, pp. 41 – 62.

Roy, S., Hussain, F., Narasimhan, K., Vengadassalam, K., and Lu, H. (2007). E-Glass /Polypropylene Pultruded Nanocomposite: Manufacture, Characterisation, Thermal and Mechanical Properties," *Polymer & Polymer Composites*, Vol. 15, No. 2, pp. 91-102.

Shao W., (2005). Polymer International, Vol. 54, pp.336-341.

Singh, A., Mukherjee, M., (2005). Effect of polymer–particle interaction in swelling dynamics of ultrathin nanocomposite films. *Macromolecules*, Vol. 38, pp.8795–8802

Sorrentino, A., Tortora, M, Vittoria, V., (2006). Diffusion Behavior in Polymer-Clay Nanocomposites, *Journal of Polymer Science: Part B: Polymer Physics*, Vol. 44, 265–274.

Vlasveld, D.P.N., Groenewold, J., Bersee, H.E.N., Picken, S.J., (2005). Moisture absorption in polyamide-6 silicate nanocomposites and its influence on the mechanical properties, *Polymer*, Vol. 46, pp. 12567–12576.

Usuki A, Koiwai A, Kojima Y, Kawasumi M, Okada A, Kurauchi T, Kamigaito O. (1995). Interaction of nylon 6-clay surface and mechanical properties of nylon 6-clay hybrid, *Journal of Applied Polymer Science*, Vol. 55 (1): 119–123.

Wu, C. L. and Zhang, M. Q. (2002). *Composite Science and Technology*, Vol. 62, pp.1327-1340.